TAMPERE UNIVERSITY OF TECHNOLOGY

PUSKAL KUNWAR

Nanofabrication using Two-photon Polymerization and Direct Vectorial Writing

Master of Science Thesis

Examiner: Dr. Juha Toivonen
Examiner and topic approved in the
Science and Chemical Engineering
Council meeting on
May 4, 2011

ABSTRACT

TAMPERE UNIVERSITY OF TECHNOLOGY
International Master Degree Program in Science and Bioengineering
KUNWAR, PUSKAL: Nanofabrication using Two-photon Polymerization and Direct Vectorial Writing
Master of Science Thesis, 59 pages, 2 appendix pages
June 2011
Major: Nanotechnology
Examiners: Dr. Juha Toivonen, Dr. Godofredo Bautista
Keywords: Nanofabrication, Two-photon photopolymerisation, Photoinitiator, Photoresist, Resolution, Vectorial Scanning.

Lithography, universally considered to be the backbone of nanotechnology, has been consistently undergoing several developments to achieve a resolution of 10 nm or less. Such resolution can be attained by using traditional electron-beam excitation and chemical protocols. Interestingly, optical lithography, which is a process of transferring features on a photosensitive material using light, has also been evolving to meet the demands of the semiconductor industry. For more than three decades, optical lithography and the semiconductor industry cooperatively work together where the former acts as the engine that powers the so called nanotechnological revolution.

Two-photon photopolymerisation (TPP), a nonlinear optical phenomenon, provides an alternative route for fabricating three dimensional (3D) nanostructures. Such a fabrication technique has outshone any other optical lithography in terms of resolution and flexibility. The resolution of TPP is characterized by the size of voxel. Moreover, the size of the polymerized spot is strongly influenced by several parameters. Carefully combining the optimal parameters (e.g., photon density, wavelength, scanning speed, material and its processing) in the experiments allows one to fully fabricate nanostructures with line widths below the diffraction limit.

In this thesis, a spin-coated negative photoresist (SU-8 5) on glass substrate is used to demonstrate nonlinear lithography. The effects of sample thickness, laser power, scanning speed were studied by using a custom-built TPP experimental setup with a Ti-Sapphire (TiSa) femtosecond (fs) laser as an excitation source. The results showed that optimal fabrication of nanostructures can be achieved using sample thickness of 5 μm, laser power of 43 mW and scanning speed of 15 μm/s. The results obtained were similar to the result mentioned in the reference 'S. Kawata, H. Sun. *Two-photon photopolymerisation as a tool for making micro-devices.* Elsevier 208-209 (2003), pp. 153-158.' The smallest linewidth drawn with these optimized parameters was 358 nm. Additionally, the aspect ratio of the sample and its reproducibility were investigated. The aspect ratio matches with the results revealed in 'H.J. Kong et al. *Ultrafast Laser Induced Two Photon Polymerization of SU-8 High-Aspect-ratio structure and nano wire*. Journal of the Korean Physical Society 54 (2009)1, pp 215-219'. Implementation of vectorial scanning was another aspect of this work. Here, the spin coated photoresist on glass substrate is guided along the fixed laser focus to photopolymerize and subsequently fabricate a plurality of nanostructures ranging from simple (e.g. lines) to arbitrary (e.g. like star, TUT emblem and maps). In future, the current workstation will be improved by introducing polarization and tailored light distribution, stimulated emission depletion (STED) concept, and the spectroscopy of photoinitiators to achieve fully controllable photo-induced processes at sub-diffraction resolution.

PREFACE

The Master of thesis 'Nanofabrication using Two-photon Polymerization and Direct Vectorial Writing' was done in optics laboratory of department of Physics at Tampere University of Technology. The work was associated with project PHORMAT and funded by Academy of Finland.

I would like to express my sincere gratefulness to Dr. Juha Toivonen for providing me opportunity to work on this topic and examining my thesis. This topic exceptionally suits my master studies and my interest. I am indebted to Dr. Godofredo Bautista for providing me tons of knowledge on the topic, answering my queries, and commenting on my manuscript. Special thanks to M.Sc. Jaakko Saarela and M.Sc. Tapio Sorvajärvi for their help in building my experimental setup. I acknowledge M.Sc. Miro Erkintalo and Antti Aalto for helping me with operating lasers. Special thanks to M.Sc. Juha Kontio and M.Sc. Milla-Riina Viljanen for providing me training for SEM imaging. I am obliged to Department of Biomedicine and Optoelectronic Research Center (ORC) for allowing using their clean room facilities.

I would like to express my humble respect and gratefulness to Professor Martti Kauranen for accepting me as a family member of Optics laboratory.

This work of mine is dedicated to my father Advocate Kul Bahadur Kunwar and mother Laxmi Devi Kunwar. I would like to show my due respect to my family for their continuous care, love and affection.

Tampere, 25th August, 2011

CONTENTS

LIST OF ABBREVIATIONS

AFM	Atomic Force Microscope
AOM	Acousto-optical Modulator
APT	Advanced Positioning Technique
FIB	Focused Ion Beam
HMDS	Hexamethyl Disilizane
IPDS	Ion Projection Direction Structuring
IPL	Ion beam Projection Lithography
LMIS	Liquid Metal Ion Source
MOEMS	Micro-Opto-Electro-Mechanical Systems
NGL	Next Generation Lithography
NIL	Nano Imprint Lithography
PI	Photoinitiator
PMMA	Poly (methyl_methacrylate)
PS	Photo-sensitizer
RIE	Reactive Ion Etching
SEM	Scanning Electron Microscope
STED	Stimulated Emission Depletion
TiSa	Titanium-Sapphire
TPA	Two-photon Absorption
TPP	Two-photon Polymerization
VLSI	Very Large Scale Integration
1PP	Single-photon Polymerization

LIST OF SYMBOLS

N_{TP}	No of molecule per unit volume in excited state
δ, σ_2^a	Two-photon absorption cross section
σ_2	Two-photon cross section for radical generation
N_{GS}	Number of molecules per unit volume in the ground state
F	Photon Flux
$\sigma^{(2)}$	Two-Photon Absorption Coefficient
R^o	Radical
M	Monomer
P^o	Growing polymer
PI*	Excited Photoinitiator
PI	Photoinitiator
D	Dose
D_p	Sensitivity for positive resist
D_p^o	Reference dose
γ_p	Contrast factor
D_g^x	Sensitivity for negative resist
Φ	Quantum Yield
ρ	Radical density
ρ_{th}	Threshold radical density
η	Efficiency for initiation process
N	Photon flux
z_R	Rayleigh length

1 INTRODUCTION

In early 2002, one of the experts of lithography, with the forecast of demise of optical lithography, said that "Without some intervention that significantly changes the way optical microscopy is practiced, a next lithography technology such as extreme ultraviolet lithography or electron projection lithography will be required to extend the road map to the 45 nm node and beyond". But within a time period of less than a decade, optical lithography has paved its way down to 40 nm or less [1].

Gordon Moore in 1965 proposed Moore law followed by the semiconductor and microelectronics Companies. This law states that the number of transistors in integrated circuits would continue to double in each technological generation. Here optical lithography plays a significant role for being able to follow the law up to this date. Martin Wegener and his group's lithographic line width of 60 nm [2], and Linjie Li and his group's achievement of resolution down to $\lambda/20$ [3] are the evidences that the above mentioned statement is true.

Development of the femtosecond (fs) laser has rapidly opened the door of multidisciplinary research in all the fields of natural science; especially in physics and more precisely in optics. Exceptional precision in time and space of the laser energy is the key feature of major application of this femtosecond laser. This development has been recognized with the chemistry Nobel Prize in 1999 [4]. The femtosecond laser has been used in high resolution imaging such as multi-photon microscopy and lithography such as two- photon photopolymerisation (TPP).

Maria Göppert-Mayer developed a theoretical model of multi-photon absorption (MPA) in 1931. This phenomenon was experimentally observed soon after the development of the laser, i.e., after three decades of the Maria's model. The process of multi-photon absorption takes place for high photon flux density. This is due to the dependence of n photon absorption to the n^{th} power of photon flux density. In the case of two-photon absorption (TPA), the probability of the absorption of the photon is directly proportional to the square of intensity of light. In the focal spot the intensity of light is highly concentrated in the small area with high spatial resolution. Employing this concept in lithography, it is possible to fabricate three dimensional objects with sub-micron resolution [5].

This thesis is concerned with TPP techniques and its resolution. TPP, a young direct laser write fabrication technique, is still in its infancy with lots of potential for future improvement. This technique allows the fabrication of three dimensional structures with the resolution less than 200 nm. In TPP, light with power above certain threshold triggers photopolymerisation. Here monomers or weakly cross linked

polymers are bonded to form a long chain of highly cross-linked polymer [5]. Resolution has been very important topic in any imaging and fabrication technique. In optical lithography, the resolution is provided by wavelength of light and numerical aperture of optics and it is limited by the diffraction of light [6].

The behavior and reaction mechanism of polymeric resist is an important topic to be addressed as the key objective of this thesis. A photopolymerisation system consists of light source, photoinitiator and monomers. Here the light source is used to expose the resist which consist of photoinitiator molecules and monomers. Photoinitiator molecules initiate a photopolymerisation reaction upon absorption of a photon [7]. Effort has been made to develop photoinitiator molecules with large cross section so that TPP is achieved with less expensive picoseconds (ps) laser or even nanoseconds (ns) laser. Monomers are small molecules which polymerize after the initiation of photopolymerisation [8].

Vectorial fabrication is the important aspect of this thesis. It is performed by utilizing the Freeman algorithm. This algorithm produces chain codes and these chain codes are used to represent boundary by a connected sequence of straight line segment of specified length and direction. The chain codes guide the laser beam in a predefined direction in order to write a structure onto the sample [9].

The main application fields of TPP are nanophotonics, microelectronics, micro fluidics, biomedicine, photodynamic therapy etc. In photonics, TPP is employed to fabricate structure like photonic crystal, planar and non-planar waveguides, Fresnel lenses, Machzehnder interferometer, micro resonator, optical data storage and so on. In biomedicine, TPP is exploited to fabricate a system for drug delivery like micro syringe, tissue scaffolds, small bone prosthesis, micro tweezers, and biosensors. In micro electronics, it is used to fabricate optical circuitry, 3D micro inductor etc. Fabrication of three dimensional micro-inductor is an example of a device which is impossible to fabricate by means other than TPP [10-16].

This thesis contains information obtained from different technical disciplines. It consists of seven chapters including the introduction. Chapter 2 describes lithography and its type. The TPP processes, material for fabrication and reaction mechanism are discussed in Chapter 3. Resolution of an instrument is its ability to distinguish two closely spaced different points. This topic is covered in detail in Chapter 4. Chapter 5 gives information about the optical setup, scanning system and fabrication methodology used in this thesis. The results of the experiments are discussed in Chapter 6. Chapter 7 concludes this work which is followed by reference and an appendix.

2 LITHOGRAPHY

Lithography is the process of patterning the substrate to define a structure in order to build a device. It is coined after two Greek names, *Lithos* and *Graphein*. Lithos is the ancient Greek name for stone and Graphein means to write. These two word literally mean 'to write on stone'. The phenomenon of transferring image drawn in limestone or wax to the printed sheet, practiced in the 17th century, is completely different to the way it is practiced today. Today lithography techniques use femtosecond laser, electron-beam, ion-beam and so forth to fabricate structures smaller than 10 nm. For this reason, lithography is considered to be the backbone of the nanotechnological revolution [17].

Lithography can be broadly divided into two types: optical lithography and non-optical (alternate) lithography. Optical lithography is the predominant patterning technique using light as a writing element which is capable of producing sub-100 nm pattern. Non-optical lithography replaces the light source with an electron-beam source, ion-beam source, X-ray source etc. and is capable of writing a structure smaller than 10 nm [18,19]. These two types of lithography are described in this chapter.

2.1 Non-optical lithography

The non-optical lithography is characterized by the irradiation source other than light. Here, the resist is irradiated by electron-beam, ion-beam, X-rays etc. Non-optical lithography, particularly electron-beam lithography, has surpassed optical lithography in terms of resolution. The resolution of sub-10 nm is achieved using this technique [19].

Electron-beam lithography is a powerful technique in fabrication ranging from micron to nanometric scale. It is the modification of the scanning electron microscopy (SEM) system and has a resolution around 10 nm. Here, electron-beam irradiates polymeric material in order to pattern the structure. The fabrication of the pattern with this technique of fabrication is divided into three processes. They are exposure of electron beam into the sensitive material, development of resist after exposure and transfer of pattern [19].

Electron gun provides a stable beam of electrons with acceleration ranging from 0.1 to 30 keV. This gun consists of three electrodes namely cathode, anode and grid electrode. The cathode is heated to produce free electrons and these electrons are accelerated towards the anode. These electrons pass through the aperture at the anode to the electron optical column. The grid electrode controls the emission current of the cathode. There are different types of electron guns namely, field emission gun (FEG), heated tungsten filament gun and lanthanum hexaboride filament gun. Among these guns, the FEG holds the better position in term of size of beam spot (the size of beam

spot being less than 10 nm) and lifetime. The electron optical column comprises of electromagnetic lenses that treat the electron beam as optical lenses treat light. The collection of the electron-beam system consists of the condenser lenses and the objective lens. These lenses demagnify the electron-beam to the final spot diameter of less than 10 nm [20]. This demagnified beam irradiates the resist to fabricate the structure. There are two approaches of fabrication: additive approach and subtractive approach. In the additive approach, the fabrication is done by deposition of the substances over the layer while in the subtractive approach the fabrication is done by removing the substances from the resist layer. Figure 1 is the example of the world's smallest nanoguitar fabricated by electron-beam lithography which is winner of an award for best scanning electron micrograph at the 41st Electron, Ion and Photon Beam Technology and Nanofabrication Conference in Dana Point, California, in May 1997 [21].

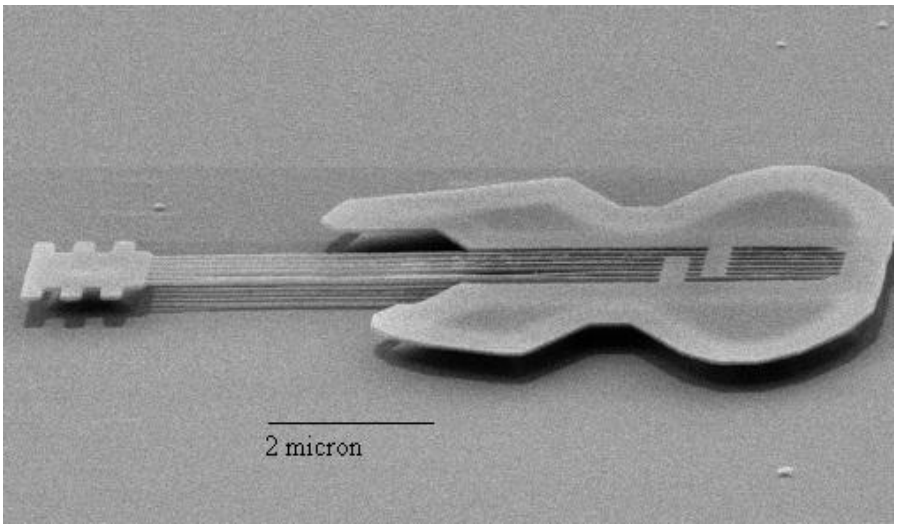

Figure 1: World's smallest guitar fabricated by electron-beam lithography. This guitar is 10 µm long, about the size of a single cell, with six strings each about 50 nm thick. The string resonates when plucked by Atomic Force Microscope (AFM) [21].

The structure fabricated with this kind of lithography can be as small as 10 nm. This technique has the ability to expose a nanometer feature without a mask. One of the key limitations of this technique is its low throughput. Pattern transfer is very difficult as the dimension of the fabrication goes down to nanometer scale. The electron-beam lithography is very expensive and the mechanics are highly complex [22].

Ion-beam lithography is another non-optical lithographic technique. Here the beam of ions is used to pattern a resist on the substrate and it is more or less similar to electron-beam technique in terms of application and feature size. They follow additive and subtractive approaches of fabrication similar to electron-beam lithography. This technique has surpassed a resolution of 100 nm [23]. Here, a mask can be utilized for the fabrication but direct writing is also possible. There are basically three ion-beam

techniques for fabrication: Focused ion-beam (FIB), Proton-beam writing, and Ion projection lithography (IPL).

FIB lithography has capabilities of writing extremely small line avoiding proximity effect. Proximity effect is a phenomenon where a developed pattern is wider than a scanned pattern due to energy deposition. This energy deposition leads to unwanted exposure**.** This is the most practiced ion-beam lithography compared to others. Here, the focused beam of slow heavy ions (e.g. 30 keV Ga^+ ions) fabricates the structures. This is a very promising method of nanofabrication with the advantage of being simple, flexible and mask-less. This lithography technique consists of Liquid ion metal source (LMIS) and FIB optics. The LMIS has high brightness which makes it possible to focus the ion-beam with the current density of order 1 Acm^{-2}. With this source, the spot size ranges from 8 nm to 200 nm. The FIB optics consists of electrostatic lens and electrostatic deflector and it is mainly concerned with focusing the ion-beam to target. This method has significant advantages over electron-beam lithography in term of resist sensitivity, back scattering and proximity effects. FIB is a useful tool for device analysis, repair and advanced specimen preparation. Nowadays it is mainly used in the semiconductor, data storage and material science industry [24].

Proton-beam writing is a relatively new approach for nanofabrication in polymeric resin such as PMMA, SU-8 and photo-sensitive glasses [25]. This technique uses high energy proton-beam which can penetrate deep into the resist. Since the proton-beam has long range and low lateral spread, it is used to fabricate structure with high aspect ratio. The probe size of proton-beam is smaller than the conventional FIB; hence the proton-beam can fabricate structure smaller than conventional FIB. The proton-beam was difficult to focus below 100 nm before the development of magnetic quadruple lens [26]. Utilizing magnetic quadruple lens, Carl Zeiss has developed Orion Plus, a proton-beam writing instrument, with resolution around 6 nm [27].

IPL technique utilizes medium energy 70-150 keV ions such as H_2^+, He^+, H^+, etc [28]. Here, ion-beam illuminates the stencil mask and electrostatic lens projects the transmitted beam onto the resist. The IPL system is also used for IPDS (Ion Projection Direction Sputtering) which means it can also be used for direct writing. Though FIB and proton-beam lithography are far more superior to IPL but this process of fabrication plays an important role in cost-effective mass production. IPL is in its early development stage and the devices are restricted to a prototype testing. This technique has the resolution less than 50 nm [29].

X-ray lithography has been practiced since the 1970s after its invention at Massachusetts Institute of Technology by H I Smith. The underlying principle of this lithography technique is to expose the X-rays on the mask which is placed at a certain distance from the resist. X-rays correspond to short wavelength region of electromagnetic radiation with very high photon energy. The best wavelength, aiding for this lithography technique, lies in spectral range at around 1 nm. There are no optics developed for focusing X-rays, hence direct writing is impossible [30].

The simple instrumentation of X-ray lithography consists of a source, a mask and a resist. The X-rays are produced by synchrotron source with enough power for the lithographic process. The mask used in this technique consists of the patterned structure. The X-rays transmitted through the mask leave the pattern on the resist. The resist should be capable of absorbing at least 10 % of the radiation [30]. With the help of this technique, it is possible to fabricate structure with line widths down to 30 nm [31]. Resolution in this case is mainly affected by the diffraction, photoelectron induced spreading and resist properties. Since the wavelength of X-rays used in this lithographic technique is around 1 nm, the effect of diffraction is low compared to optical lithography [32].

2.2 Optical lithography

Optical lithography is a process of patterning photolithographic material with the help of light. It is a major tool for VLSI production and it has been dominating the field of semiconductor fabrication for decades. In this technique, a light sensitive polymer, namely photoresist, is exposed by light and developed to form various structures on a substrate. This complex fabrication procedure involves different physical and chemical processes like photoresist processing, optical exposure and imaging, pattern transfer and photomask designing [33].

Optical lithography can be broadly divided into two types, namely mask-based photolithography and mask-less (direct writing) photolithography. In mask-based photolithography, the fabrication is done utilizing a photomask. The light shines onto the photomask and the photomask is patterned in such a way that it blocks the light in some areas and lets it pass in others. This results in irradiation of resist in the desired area. This technique has high throughput and it is relatively cheap [34]. The mask-based optical lithography can be divided into mask aligning lithography and projection lithography.

In the case of mask aligning lithography, the photomask is placed between the sample and the light source. The size of the pattern formed is equal to the size of pattern in the photomask. The mask aligning lithography can be further divided into contact and proximity lithography. In the contact lithography technique the photomask is in contact with the resist. If pressure is applied between the photomask and the resist, then it is hard contact lithography and if the pressure is lifted, then it is soft contact lithography. There is a small gap between the resist and the photomask in proximity lithography. This gap greatly affects the quality of the patterned structure. The quality can be enhanced by minimizing this gap. As there is no contact between the photomask and the substrate, the proximity lithography has the advantage of increased photomask life time [35].

In the case of projection lithography, the photomask still occupies the place between the sample and the light source and in addition there is a focusing lens in

between the sample and the photomask. The projection lithography can fabricate the same sized structure as mask as well as smaller than the mask. The dependence of the distance on the gap between the sample and the photomask on resolution is overcome by this lithographic technique. Though 1:1 projection lithography can replace the mask alignment lithography, it is not adequate for growing challenges of fabrication especially in IC manufacture. Thus 5:1 lithography technique is implemented which diminish the fabricated structure 5 times less than the photomask size [35].

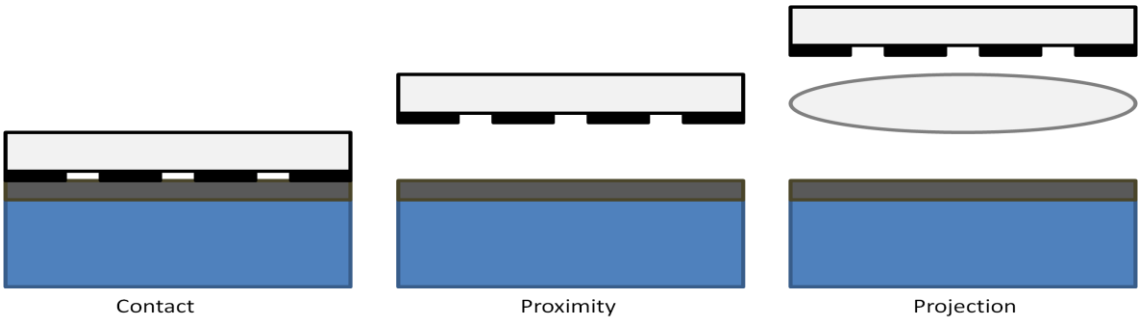

Figure 2: Types of exposure system in mask based photo-lithography. In the case of contact lithography the mask is in contact with photoresist. In the case of proximity lithography the mask is at certain distance from the resist which significantly decreases the resolution. In the case projection lithography the lens design is added in between the photomask and the substrate.

The mask-based lithographic system is limited in resolution and does not help in three dimensional fabrications. This technique is not flexible enough as it is based on utilization of photomask. These photomasks are relatively expensive and must be durable and immune to frequent handling and repeated use. The other problem in utilizing a photomask is foreign particles attaching to the photomask which affects the pattern duplication. These limitations in mask-based lithography are overcome by the mask-less lithography technique. In the mask-less lithographic technique, the radiation is not projected with the help of the photomask in order to irradiate the resist but the radiation is focused to form a narrow beam. This beam is employed to write the structure on the photosensitive emulsion. Here the sample is scanned by moving the beam using a galvanic mirror or the beam is fixed in one position and the sample is moved across x, y and z directions [36]. Thus this system completely removes the photomask from the optical lithographic technique.

There are various types of optical lithography practiced today. Some of them are ultraviolet lithography (UVL), extreme ultraviolet lithography (EUVL), stereo lithography and two-photon lithography. UV lithography is the most commonly used photo-lithography technique. This lithography technique uses ultraviolet light for exposure. The basic principle is to shine the UV light through the mask into the resist or focus and scan the UV beam into the resist. The process of fabrication includes: substrate cleaning, resist coating, pre-bake exposure, exposure, post-bake, development and pattern removal. EUVL uses light of extreme ultraviolet wavelength around 13.5 nm. It is not possible to use refractive optics in this technique of lithography as almost

all materials are strong absorbers of light in the extreme ultraviolet wavelength region. Hence, the refractive optics is replaced by reflective optics. The EUVL system consists of source, illumination optics, a mask, an objective and photoresist. The source used earlier was SR (Synchrotron radiation) source. This source couldn't provide enough throughputs so it is now replaced by the Laser produced plasma (LPP) source. The EUV mask consists of low thermal expansion glass substrate, and multi-layer absorber pattern of Mo/Si. This multi-layer absorber pattern of Mo/Si is suitable for obtaining high reflectivity. The exposure system consists of the objective lens made by the multi-layer coated mirror known as Bragg's reflector. The resolution of the EUV technique is around half the wavelength of light used [37].

Stereo lithography, rapid prototyping technology, is method of layer by layer fabrication of three dimensional objects. This method is employed to fabricate all kinds of objects despite their complexity. It is used in various fields of application especially in manufacturing industrial products. The stereo lithography system consists of the following essential elements: CAD design for slicing, two dimensional patterning functions, laser scanning and controlling system with monitoring device [38]. This technique utilizes CAD (Computer-Aided Design) and CAM (Computer-Aided Manufacturing) for slicing the three dimensional objects into many two dimensional planes. The UV laser beam draws the pattern corresponding to the lowest plane of sliced three dimensional objects on the thin layer of resin. Now either the beam is pushed up or the table is pulled down and the new layer of resin is poured onto the first patterned structure. The exposure is done again. This procedure is repeated for all sliced plane [39].

Micro-stereo lithography is a technique of sub micro-lithography using the principle of conventional stereo lithography. The only difference is the dimension of the fabricated structure. This technique follows the additive approach of fabrication. The main advantage of using this technique is the rapidity of fabrication. The three dimension patterning can be done within a short period of time despite its complexity [40]. Figure 3 depict the working principle of stereo lithography.

The next approach of optical lithography is two-photon lithography which is the three dimensional approach of nano-fabrication. The monomer in liquid or gels, along with photoinitiators, are irradiated by focused laser beam to create three dimensional structures. As this thesis mainly focuses on two-photon photopolymerisation and its resolution, this topic is described in more detail in next chapter.

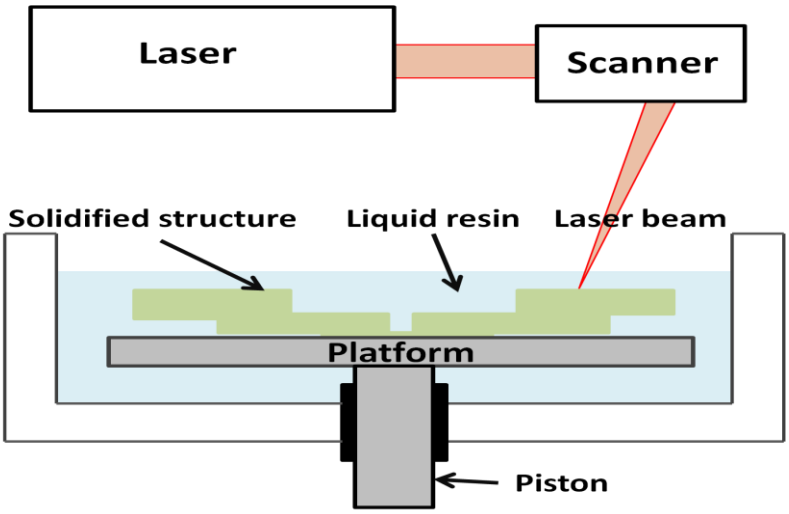

Figure 3 : Illustration of the principle of stereo lithographic technique used in micro-fabrication. The liquid resin over the platform is irradiated by laser and the laser beam is scanned by scanner for fabrication of a single layer. The piston is moved down and the fresh resin over the solidified resin is again irradiated. This process continues until the whole structure is fabricated.

2.3 Optical lithography and semiconductor industry

Optical lithography is a basic tool for IC fabrication. It is considered as industrial workhorse in semiconductor engineering and it has been meeting the ever tightening requirement of semiconductor industry. There are various physical and chemical phenomena that are taking place on a semiconductor (e.g. silicon substrate) during the fabrication of integrated circuit. These varieties of processes can be divided into film deposition, patterning and semiconductor doping. Optical lithography plays an important role in these fabrication procedures of integrated circuits. It is used to create billions of transistors and built them into a complex circuitry that subsequently built modern micro-electronic devices [41].

Line width control (resolution) and the performance are the two important aspect of lithographic technique in the semiconductor industry [41]. The strength of optical lithography is its large degree of parallelism with high throughput and low cost. Optical lithography can pattern 200 wafer levels per hrs at resolution of 45 nm which means that the throughput is very high (around $2*10^{12}$ pixels per second). This capability of optical lithography surpasses other lithographic techniques in terms of throughput. Resolution in optical lithography is given by $R=k*\lambda/NA$. Here k, λ and NA are proportionality factor, wavelength of light and Numerical aperture respectively. The NA has increased from 0.5 to 1.35 due to introduction of immersion objectives, λ has reduced from 395 nm to 193 nm and k has been reduced from 0.7 to 0.27 which has dramatically enhanced resolution to 45 nm. There has been much effort made to reduce the resolution to 23 nm. The idea is to reduce the value of k from 0.25 to 0.125 by the

process known as double patterning. This is the process where several thin film deposition, etch steps and additional lithography steps are followed to fabricate structure with resolution down to 23 nm [42]. If we rely on the information provided by Wikipedia on the topic '22 nanometer', there has been many claim made for extension of optical lithography to 22 nm. IBM, its partner AMD, STMicroelectronics, Toshiba and the college of Nano-scale and engineering claimed to develop SRAM using 22 nm technology. Intel has showed 22 nm wafers and has announced its first 22 nm microprocessor on May 2, 2011.

Although there is extensive research going on in alternate lithography but optical lithography still remains the main weapon used in manufacturing semiconductors at large scale. As mentioned earlier there has been drastic enhancement in resolution in recent days. The resolution of 16 nm is thought to reach at the end of 2016 and 11 nm within a decade which would push optical lithography much closer to electron microscopy in term of resolution [42]. This would help to fabricate billions of transistors in one chip.

3 Two-photon photopolymerisation

Two-photon photopolymerisation is a three dimensional approach of nanofabrication where monomer in liquid or gels along with photoinitiators are irradiated by focused laser beam. This is the serial approach of three dimensional fabrications. The theory of multi-photon appeared 40 years ago but TPP was established as a lithographic technique in 1997 by S. Kawata and his group [43]. Though other lithographic techniques like electron-beam lithography, ion-beam lithography surpass this technique in terms of resolution but this is the strongest tool for three dimensional fabrications [44]. The background of the two-photon absorption principle and influence of photoinitiator is described below which is followed by its advantage in three dimensional nanofabrication.

3.1 Two-photon absorption

Two-photon absorption (TPA) is a non-linear optical phenomenon. In this process electron transition from ground to excited state takes place by the simultaneous absorption of two photons. The excitation of the atom or molecule occurs from the lower quantum state to excited state of same parity. This transition depends on absorption cross section and photon energy. The theory of two-photon absorption was proposed by Maria Göppert-Mayer in her PhD thesis in 1931 [45]. This effect was experimentally observed by Kaiser and Garrett after the demonstration of the first working laser in 1960 [46].

Figure 4 is a simple Jablonski diagram of single-photon absorption (1PA) and two-photon absorption. In 1PA (left), single photon of energy $h\upsilon_a$ mediate the optical transition from ground state (S_0) into the electronically excited state. This is followed by non-radiative relaxation and consequently spontaneous emission (fluorescence). In TPA, two photons with energy $h\upsilon_b$ are simultaneously absorbed by molecule in very short interval of time and the molecule gets excited to the electronically excited state (S_1). This is followed by non-radiative relaxation and consequently by spontaneous emission. Each individual photon does not carry enough energy corresponding to the S_1 state but their sum does carry enough energy to excite the molecule to the S_1 state [2,13,46,47].

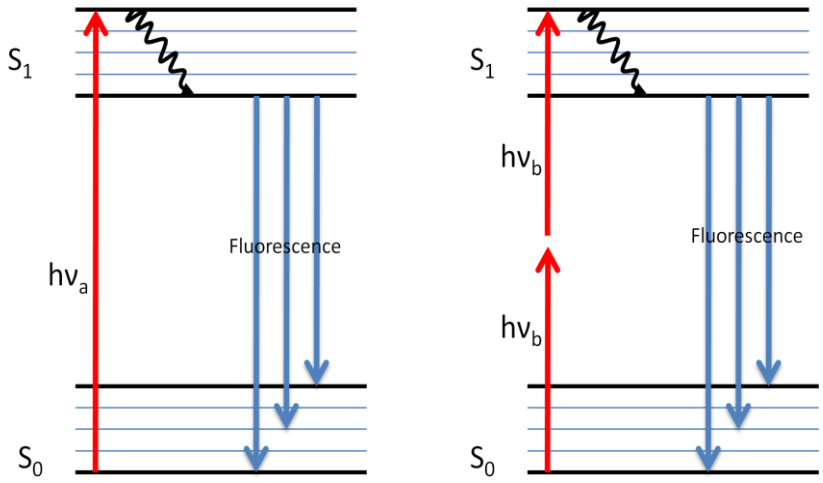

Figure 4: Illustration of excitation of photoinitiator molecule from ground to excited state by single (left) and two-photon absorption (right) [47].

Resin used in TPA should be selected carefully considering the parameters like photoinitiators, monomers, oligomers, photosensitizer or co-initiators. Much effort and money is being poured into manufacturing the noble photoinitiator. The cross section of photoinitiator plays an important role in TPA. It is an effective area provided by the photoinitiator molecule for incoming photon interaction in order to achieve a simultaneous absorption of two photons. This quantity is measured in GM units where one GM is equal 10^{-50} cm^4s per photon. Most of the commercially available resists have a small TPA cross section. This means that the probability of the interaction of the photon with the photoinitiator is low. Hence large photon flux is required to achieve the photopolymerisation. There has been considerable effort aimed at increasing the cross section of the photoinitiators to prepare the noble photoresist. The laser power and exposure time is fairly reduced for larger cross section photoinitiators. It is thought possible to use a low cost micro laser for nanofabrication using the photoresist with larger cross section photoinitiators [47].

In the case of lPA, the molecules are excited throughout the beam path as shown in the Figure 5. This is not the case with the TPA where the molecules close to the focus only get excited as the excitation rate depends on the square of intensity of light as shown in the following equation [46,47]:

$$R = \frac{\sigma^{(2)} I^2}{\omega} \quad \text{.....(2)}$$

where $\sigma^{(2)}$ is TPA coefficient, ω is laser frequency and I is laser intensity.

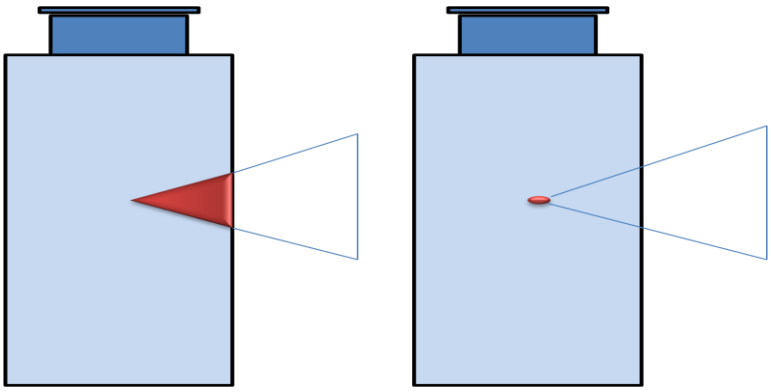

Figure 5: Illustration of single photon absorption (left) and two-photon absorption (right) in fluorescent dye solution. In the case of single photon absorption, excitation results in absorption along the entire path of the laser beam in the cuvette. In the case of two-photon absorption, excitation of two photons is confined to focal volume of laser light [47].

The penetration in TPA is high when compared to 1PA. This is more clearly shown in Figure 6. The solution is a strong absorbing solution (highly concentrated fluorescent compound). Excitation is seen on the right wall of the beam for the 1PA which shows that the beam is strongly absorbed and attenuated as it goes to the left. The two-photon excitation occurs at the middle of the sample. This reveals the high ability of penetration in TPA which makes it capable of accurate three dimension focusing [47]. For TPA to occur at the middle, the excitation is compressed spatially using lens focusing, temporally by using pulsed femtosecond lasers. Use of longer wavelength also aids in minimum scattering of light.

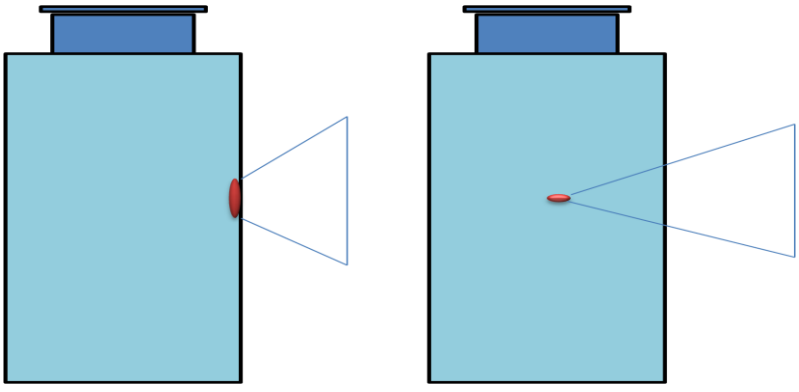

Figure 6: Illustration of single-photon (left) and two-photon (right) process of penetration in concentrated solution of fluorescent material. In the case of single-photon, excitation results in absorption by surrounding medium before beam reaches sample. In the case of two-photon absorption, excitation allows for the penetration through the material followed by the absorption of two photons by sample [47].

In single-photon polymerization (1PP) process, an initiator molecule absorbs one UV photon to form a radical. This radical reacts with the monomer and initiates polymerization. The UV photolithography and stereo lithography are examples of 1PP. As discussed above in 1PA, the UV light is absorbed by the resin within first few micro-meters. Hence 1PP is planar process of writing which is restricted to two dimensional fabrications. In TPP, an initiator absorbs two near infrared photon simultaneously through non-linear absorption. This absorption of photons leads to production of the radical. This radical reacts with the monomer to initiate polymerization. For the polymerization process to occur, the photon density should exceed a certain threshold value. The cross section of TPA is smaller than for 1PA. For this reason, TPP is possible only if the excitation beam intensity is in the order of TW/cm^2. The development of femtosecond laser makes TPP possible as the peak power of this laser is extremely high. As soon as the photon density exceeds the threshold value of polymerization, the laser spot is moved three dimensionally through the volume of the resist in order to write a structure. This is done either by scanning the laser beam via a galvanic mirror or by moving the sample-stage by a piezo controller [47].

There are several advantage of TPP compared to 1PP. The polymerization is initiated within the volume of resin; hence TPP is three dimensional fabrication process. In 1PP three dimensional structures can be fabricate by working layer by layer. However this limits the resolution and is not flexible for rapid single step fabrication. In 1PP, the polymerization is suppressed by the oxygen on the surface of the molecule. The oxygen quenches the radicalized molecule and suppresses the polymerization process. In order to achieve an optimized resolution, the 1PP process has to be performed in an inert gas atmosphere. This drawback can be overcome in TPP as we work in the volume rather than the surface. Resolution in TPP is enhanced compared to 1PP as the two-photon excited spot is smaller than the single-photon excited spot [47]. This is explained in Section 4.2.

3.2 Photopolymerisation

Photo induced polymerization is a chain process of bond formation initiated by light. In this mechanism, the light beam starts the photo physical and chemical reaction in organic material forming new polymeric material. Simply it can be defined as the reaction of monomer or macromer to produce polymeric structures that are induced by light in UV, visible to IR spectral region. Monomer and Oligomer are basic component of photoresist. Upon light excitation, these monomers and oligomers solidify by two mechanisms: polymerization and cross-linking. Polymerization is the process of the chain reaction by which macro molecules are created. The case is different with the cross-linking where there is formation of cross-links with the chemical bonds. The difference in photopolymerisation and cross-linking can be described in term of quantum yield. (Quantum yield is ratio of number polymerized monomer units to

number of photon actually needed for the polymerization.) In the case of cross-linking, there is requirement of a photon for addition of each monomer unit. The quantum yield is less than one in this case. On the contrary the quantum yield can reach several thousand as the photopolymerisation occurs via chain reaction [48].

Photopolymerisation has various applications in lithography, photonics, Opto-electronics, micromachining, chemistry, medicine, material science, biomedicine etc. Integrated circuit (IC), recording media, surface relief grating, anisotropic material, clays nanocomposites, micro resonator, micro assemblies, micro optical component like photonic crystal, micro lenses, gratings, zone plates, waveguides, interferometer, microfibers, 3D micro inductors, micro syringe, bone and tissue implants and scaffolds have been already fabricated using photopolymerisation [14,15,49,50].

3.3 Photopolymerisation mechanism

The photopolymerisation starts with the initiation of polymerization in a photo-sensitive material by photoinitiator. This photo-sensitive material exhibits high absorption at a specific wavelength. The initiating species can be free radicals, cations or even anions and weak bases. The free radical polymerization dominates over the cationic and anionic photo-initiation. The reaction mechanism is completed mainly in four phases [48]. They are initiation, association, propagation and termination.

Upon absorption of a photon of suitable photon energy, the photoinitiator (PI) transforms itself into a reactive initiating species known as a free radical or cationic radical (R^0). These reactive species associate with monomer (M) in order to produce monomer radical (RM^0). The RM^0 combines with new monomer forming a long chain. This process of addition of the monomer in the continuously growing polymer is known as propagation. This process of propagation terminates when the two chains meet and react at their radical ends. A summary of photopolymerisation mechanism is given below [48]:

$$\text{Photo-initiation} \qquad PI \xrightarrow{\lambda} PI^* \rightarrow R^0$$

$$\text{Association} \qquad R^0 + M \xrightarrow{k_1} RM^0$$

$$\text{Propagation} \qquad RM^0 + M + \cdots \xrightarrow{k_p} RM^0{}_n$$

$$\text{Termination} \qquad RM^0{}_n + RM^0{}_m \xrightarrow{k_t} RM_n + RM_m$$

The photopolymerisation system consists of source of light, photoinitiator and monomer. The light sources used in photopolymerisation are UV lamp, plasma arc lamp, halogen lamp, light emitting diode lamp and many other laser lamps. PI is defined as a molecule or group of molecules that initiates polymerization upon absorption of light. In any photo curable system these PI affects curing speed and cost of photo resist.

PI induces polymerization in two ways either directly or by the help of photo-sensitizer molecules (PS). The PS molecules first absorb the photon energy and later transfer to PI. In case of choosing PI, care should be given that the emission wavelength of light source should match the absorption properties of PI molecule. There are mainly three mechanisms of photo-initiation. These three mechanisms are free radical, cationic polymerization and anionic polymerization. The free radical system is classified as cleavage (type-1) or H-abstraction (Type-2) initiation. When the compounds like benzoin and derivatives (e.g. benzil ketals, acetophenones) absorbs light they undergo alpha cleavage to generate free radicals which initiate polymerization. Cationic photoinitiator gives acidic species when it absorbs light. The acidic species associate with monomer to initiate polymerization. Similarly anionic initiating species gives anion to initiate polymerization upon absorption of light [50].

The polymerized structure properties such as adhesiveness, mechanical strength, degradation rate etc. depends on the monomer or macromer. Thus, care has to be taken in selecting suitable monomer for appropriate application of polymerized structure. The common example of monomers are (di)methacrylic or (di)acrylic derivatives of poly(ethylene glycol), urethanes, polysaccharides, dextran, 88 collagen, hyaluronic acid, diethyl fumarate, poly(propylene fumarate) and many others [51].

3.4 Photoresist and its properties

A photoresist is a light-sensitive chemical substance. They are used in different industrial processes such as photolithography and photoengraving to form patterned structures on a substrate. The photoresist material consists of base resin (monomer which is responsible for structural properties), a photoactive compound (PAC which is responsible for initiation of photo polymerization reaction) and a solvent [52].

Photoresist materials are divided into two groups, namely positive and negative resist. A positive resist is a type of photoresist where the exposed part of resist is washed out by photoresist developer. The unexposed part of resist remains insoluble to the photoresist developer. A negative resist is a type of photoresist where the unexposed part of the resist is washed out by photoresist developer. The exposed part of resist remains insoluble to the photoresist developer. The negative photoresist is further divided into solid negative photoresist and liquid negative photoresist. Solid negative photoresist are epoxy based cationic photoresist producing acidic radical due to light exposure while liquid resist are commonly acrylate based, organically modified ceramics. Figure 7 shows the classification of photoresist material [53].

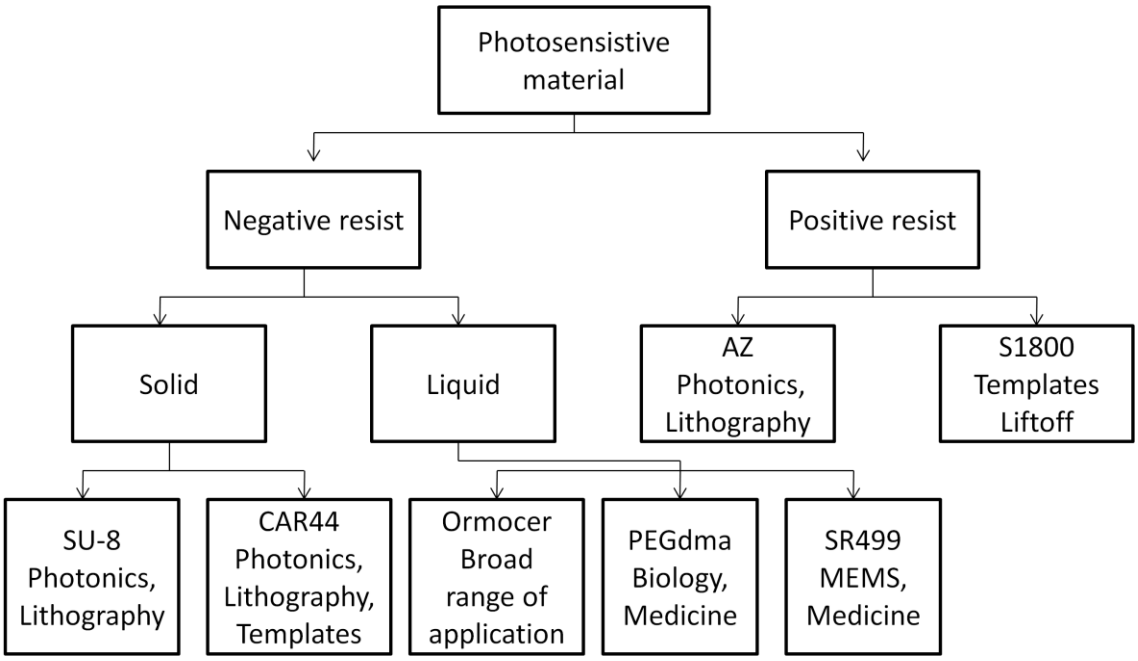

Figure 7: Classification of photosensitive material into positive and negative photo-resist and its corresponding branches [53].

There are certain parameters that affect the properties of photoresist. During the exposure all the radiation is not incident on same angle. There is scatter of the energy when the radiation reaches to resist through the wafer. The development process depends on time which means that the developed resist is not removed instantaneously. These facts affect the fabricated structure. We can mostly notice this kind of distortion in vertical side wall where the wall is not perfectly vertical as shown in the Figure 8.

The curves shown in the Figure 8 are known as exposure response curves. These curve measure the amount of remaining resist on the wafer after exposure and development as the function of dose (D). The slopes for the two tones of resist are opposite. This is because positive resist tends to increase its solubility while negative resist decreases its solubility upon the exposure of radiation [54].

In the case of positive resist, the dose required to completely clear out all the resist is defined as the lithographic sensitivity which is denoted by $D_{p.}$ The dose at which the developer starts clearing the resist is D_p^o which is known as the reference dose. The reference dose and the sensitivity helps to define the resist contrast factor (γ_p) which is given by Equation (3). This contrast factor describes the sharpness of pattern in the resist. The larger the contrast factor, the sharper the structure. This value ranges from 2 to 4 [54].

$$\gamma_p = \frac{1}{\ln D_p - \ln D_p^o} = \left[\ln\left(\frac{D_p}{D_p^o}\right)\right]^{-1} \quad \text{.....(3)}$$

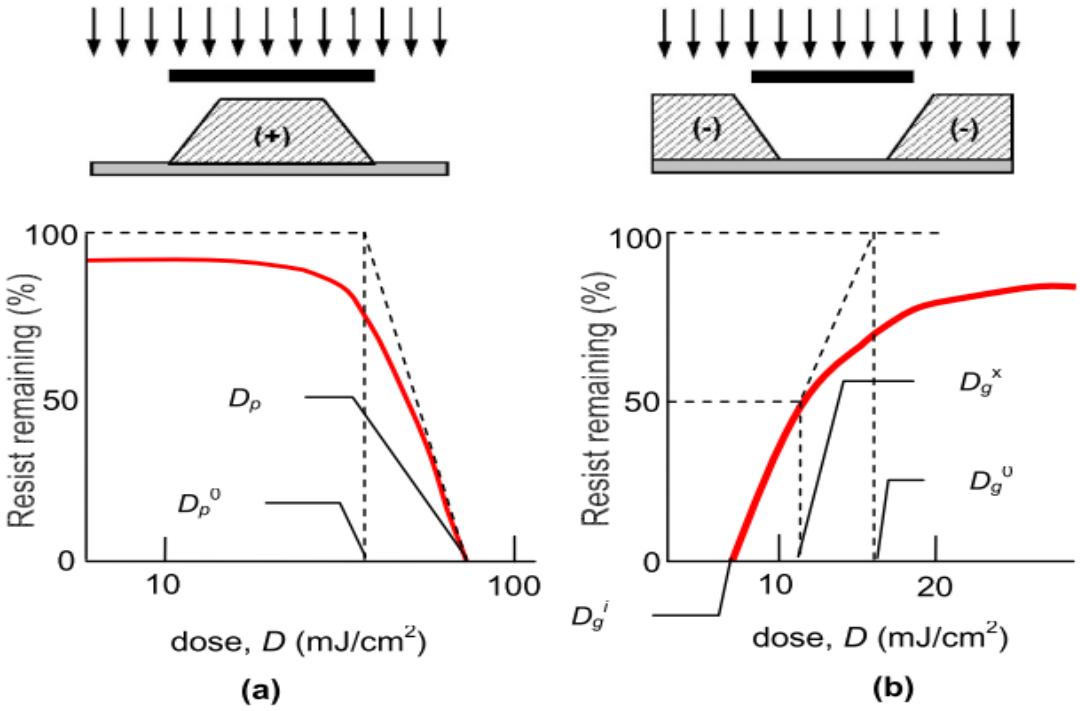

Figure 8: Illustration of resist profile and exposure response curve for a) positive resist and b) negative resist [54]

In the case of the negative resist D_g^i is the critical dose to start the polymerization where the solubility of the resist starts to decrease. Entire layer is polymerized with the dose D_g^o . Sensitivity in this case is different than positive resist. The sensitivity for negative resist affects optical resolution after development. It is denoted by D_g^x. It is typically at 50-70 % of the original thickness remaining after development. Contrast (γ_p) in this case is around 1.5 and is given by the equation below [54].

$$\gamma_p = \frac{1}{\ln D_g^o - \ln D_g^i} = \left[\ln\left(\frac{D_g^o}{D_g^i}\right)\right]^{-1} \quad \text{.....4}$$

The photochemical quantum efficiency (Φ) is defined as the ratio of the number of molecules that react to the number of photon required to accomplish that event. This quantity is also known as intrinsic resist sensitivity. The quantum yield for negative resist ranges from 0.5 to 1 and 0.2 to 0.3 for positive resists. This represents how sensitive a resist is to exposure and subsequent development [54].

Resolution in optical lithography depends upon the resolution of optical exposure system, molecular weight, molecular weight distribution, resist thickness, development condition, pre- and post-bake temperature etc. It is often easy to obtain a high resolution on a thin layer of resist. The exposed resist shouldn't be over- or under-developed as it affects the resolution. Post-bake and pre-bake temperature should also be optimized [55].

The exposed resist should be thermally stable so that the temperature doesn't affect the structure. Good resists should possess the property of stability against

chemicals. They shouldn't be affected by acids and bases. They should only show response to their developer. The developed resist should be mechanically strong and hard. Swelling occurs in some of the negative photoresist. Photoresist should not swell while treated with different chemical or by any other means [55].

Viscosity defines the thickness of the resist layer onto the substrate. For photoresist with high viscosity it is difficult to obtain a thin resist layer. Higher viscosity also limits the evaporation of the resist. Even at the same spin speed the thickness of the resist layer is different for old and new resin due to the change in viscosity. Every different resin has a specific lifetime as photoactive compound degrades with time. The limitation of the resin age is also due to evaporation of solvent. Certain resists should be stored in low temperature as they might change the property at room temperature. Resists are sensitive to ambient light so they should be stored in a dark place [56]. Table 1 compares the properties of positive and negative resists.

Table 1: Comparison of properties of negative and positive photo resist [56]

Photoresist properties	**Positive resist**	**Negative resist**
Adhesion	Average	Good
Sensitivity	Fairly low	High
Contrast	High	Low
Cost	Fairly expensive	Less expensive
Developer	Aqueous based	Solvent
Ambient oxygen	No	Yes
Etch selectivity	High	Low
Swelling	No	Yes
Thermal stability	Good	Average

3.5 Photoresist processing

The preparation steps for any typical photoresist processing include substrate preparation, photoresist spin coat, pre-exposure bake, exposure, post-exposure bake, development, post-development bake and chemical etching and stripping. The first step is substrate preparation where the substrate is cleaned to remove contamination, dehydrated to remove water and treated with adhesion promoter. The first process in substrate preparation is cleaning. It is performed by organic solvent like Acetone or Isopropanol. The dehydration process is usually performed by baking at temperature of 200-400^{o}C for up to 60 minutes. Adhesion promoters are chemical substances which improve the adhesion of the photoresist material to the substrate. They react chemically

with the surface silanol to replace OH group. Silanes often used for this purpose are hexamethyl disilizane (HMDS). Piranha solution can also be used as adhesion promoters. The treatment with piranha leaves the hydrogen moieties onto the surface. This is sometimes followed by Reactive Ion Etching (RIE) cleaning [57]. This ensures cleaning by chemically reactive plasma generated by an electromagnetic field under low pressure.

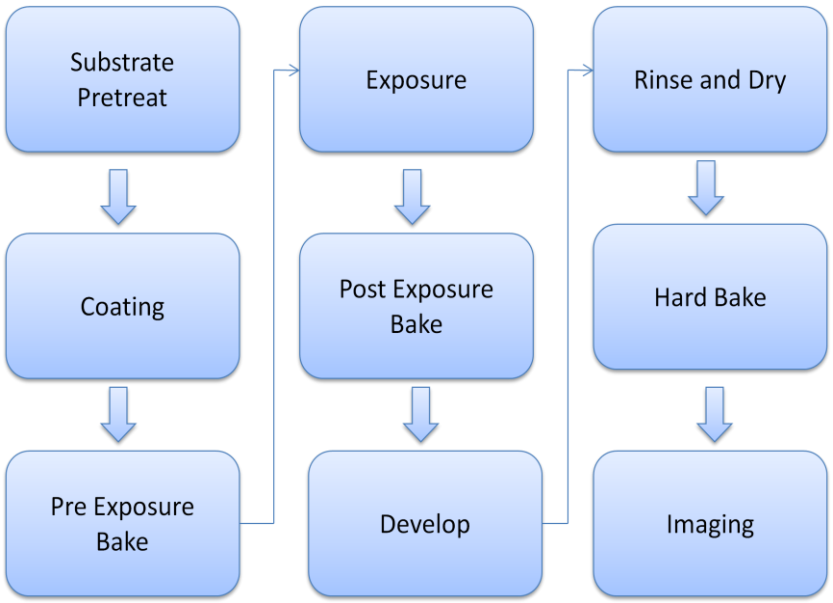

Figure 9: Schematic illustration of photoresists processing from substrate preparation to imaging of fabricated structure. The processing steps follow sample cleaning, photoresist spin coat, pre-exposure bake, exposure, post-exposure bake, development, often post-development bake and imaging.

The second step is photoresist coating where the substrate is coated with the uniform layer of resist. The thickness of the resist is controlled with spinning speed. The uniform coating can be achieved by pouring resist onto the wafer and spinning it at the desired speed for the desired amount of time. Thickness control, uniformity and low defect density are the key factors that require attention while coating. The spinning process can be static dispense where the wafer remains stationary and resist is dispensed or the dynamic dispense where the wafer is spun. The basic principle behind the photoresist spin coating is the centrifugal force that pushes the resist towards the edge opposed by the frictional force of viscosity. These forces balance each other to give resists a certain thickness over the substrate [57].

The next step is pre-exposure bake which is the process of heating the resist in order to remove excess solvent from the resist. This process stabilizes the photoresist. At room temperature the evaporation takes place continuously every moment which changes the property of resist. After the pre-exposure bake, the film thickness is reduced, post-exposure and development properties are changed and adhesion is improved. Finally the film becomes less tacky which decreases the possibility of contamination. At the same time there are negative effects of the pre-exposure bake.

The photo-active compound may start decomposing at a temperature greater than 70^{o} C. Other component of resist may oxidize and cross-linking may occur due to pre-exposure baking [57].

The pre-exposure bake is followed by alignment and exposure. The underlying principle of exposure is to change the solubility of the resist to the developer upon the exposure of light. Thus the light energy that is incident on photoresist changes the solubility of the resist to a particular developer. In masked-based exposure the light is shone into the mask with desired pattern. The light that enters through the mask leaves the pattern on the resist. Another approach of exposure is direct-laser writing. Here, the beam is focused into the sample and the sample holder or the beam is moved in x, y and z directions. In other words, the motion of the sample holder with respect to a fixed laser focus or a scanning laser beam impinging on a fixed substrate is programmed to transfer a desired pattern on the photoresist. This step is followed by the post-exposure bake. This process is meant to smooth out the standing wave ridges which cause diffusion of photoactive compound. The same effect mentioned in the pre-exposure bake applies to the post-exposure bake. Optimizing baking temperature is also critical issue here [57].

Development is the next process after the post-exposure bake. This is one of the most critical steps in photoresist processing. Here, the developer of the resist is used to wash the exposed part in positive tone resist and unexposed part in negative tone resist. This is an important step as the resist developer interaction determines the shape of the photoresist pattern. The simple development process starts by pouring the developer into the decanter. This is followed by placing the wafer into the decanter. The decanter is shacked gently. After developing the wafer for the desired amount of time it is washed and dried. There are other methods of performing development and they are spin development, spray development, and puddle development. In the case of spin development, the wafer is spun and the developer is poured onto rotating wafer. Wafer is rinsed and dried while spinning. The spray development process is similar to spin development process but the developer is sprayed rather than poured. Developer is poured into slowly spinning wafer and stopped for development duration in puddle development [57].

Sometimes the development step is followed by the post-development bake. This hardens the final resist pattern. This hardening facilitates the etching and striping steps. Exposure of high intensity deep UV light cross links and hardens the fabricated structure. Plasma treatment and electron-beam bombardment are also used to harden the pattern. The post-development bake is followed by etching and stripping. This is process of pattern transfer and lifting off the structure from the substrate [57].

3.6 Examples of photoresist

There are many types of photoresists that are commercially available. The photoresist can also be synthesized in a laboratory as per needed. Below is the brief description of a few photoresists which are commercially available. Among the mentioned photoresists below, SU-8 is used in this thesis work.

The SU-8 is an epoxy-based negative photoresist which is highly transparent, and functional. It is sensitive to light near the UV region. It is complex chemical compound which contains an oligomer and a photo-acid generator. The oligomer is Bisphenol A Novolak epoxy and the photo-acid generator is triarylsulfonium hexafluroantimonate (up to 10 wt%). The chemical structure of SU-8 is shown in Figure 10 [58].

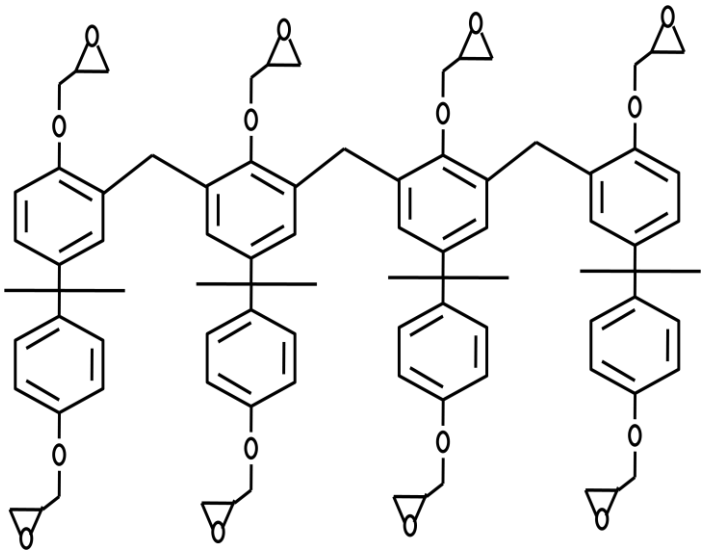

Figure 10: Chemical structure of the Bisphenol A Novolak epoxy oligomer contained in SU-8 formulations [58].

SU-8 is usually designed for micro-machining and other micro-electronics applications. It has a wide application in optics, electronics, biomedicine etc. It is also remarked with excellent thermal and chemical stability which makes it suitable for permanent use application. It has high aspect ratio which can be greater than 20. The thickness of resin ranges from 1 to >200 um with a single spin coat process. SU-8 is frequently exposed with electromagnetic radiation near UV (350-400nm), but this can also be exposed using e-beam or X-rays. After the exposure, the cross-linking procedure takes place in two steps. First there is formation of strong acid during the exposure process followed by acid initiated thermally driven epoxy cross-linking during the post-exposure bake step. Normal processing of SU-8 is processed as spin coat, soft bake, expose, post exposure bake, and develop. Detailed process is described in section 5.3. The SU-8 developer is 1-Methoxy-2-propyl acetate which is commonly known MR-Dev 600 [59].

Polymethymethacrylate (PMMA), is a polymeric positive resin which is useful for high resolution lithography. PMMA can also be used as a negative photoresist [60]. PMMA is well suited for many imaging and non-imaging microelectronics applications. This photoresist is not only suitable for photolithography but also for electron-beam lithography and X-ray lithography. It is also used for coating for wafer thinning, as bond adhesive and as a sacrificial layer. It can be purchased in wide range of variety and dilution. It has good adhesion to most substrates. The processing guide line is similar to the SU-8 sample starting from substrate cleaning to development of the resist. Microchem also offer copolymer which is mixture of PMMA and methacrylic acid (8.5%). This can be combined with PMMA in bilayer lift off resist processes. They are formulated in the Ethyl lactate solvent and available in wide range of thickness. The applications are quite similar with PMMA. They can be used with multilayer T gate processes, direct write electron-beam process, laser based lithography and device based wafer thinning, etc [61].

The SCR 500 is the urethane based resin manufactured by Japan Rubber Co. and is widely used for three dimensional microfabrications. It is composed of a mixture of benzoyl cyclohexanol and morphino amino ketones [62]. To improve and initiate TPP, photo-sensitizer (TP-Flu-TP", 0.1 % wt) can be added. The chemical formula for this photo-sensitizer is $C_{81}H_{80}N_2O_2$. Unlike the SU-8, the SCR does not need pre-exposure baking and post-exposure baking. Thus the fabrication process includes only coating, exposing and developing. The SCR 500 is more concerned with enhancing resolution. Takada et al has reduced the finer structure to 65 nm using this photoresist with the addition of a radical quencher. Though the resolution is enhanced, but the aspect ratio is very poor in case of this resist [63].

The Ormocer is inorganic-organic negative photoresist which is a good candidate for electro-optical application. This resist was first manufactured at Fraunhofer Institute with the original name Organically Modified Silicate. The inorganic backbone of the Ormocer is formed by sol-gel chemistry which contains cross-linking organic side groups. It is thermally, mechanically and chemically stable. It combines the property of several material classes. It is optically transparent, non-crystalline. It is viable for a wide range of applications. Fabricated structure using Ormocer resist have low polymerization shrinkage, minimum free residual monomer, and are biocompatible. This makes them ideal resist for fabricating tissue scaffold. They are used in coating of many substances, dental filling composites, many medical applications, optics and photonic, biosensors etc. This resist is developed by 4-methyl-2-pentanone. The commercially available developer for Ormocer is Ormodev which is manufactured by Microchem [64-66]. Table 2 lists the commercially available photoresist material with their types, preparation and post processing procedure.

Table 2: Commercially available photo resist with their types, preparation and post processing procedure.

Resin	**Type of material**	**Preparation**	**Post processing**
SU-8	Epoxy (2-step reaction)	Use directly (Microchem)	(1) Post-bake, (2) Washout in special developer
SCR 500	Urethane acrylate	Use directly (Japan Synthetic Rubber Co., limited customers)	Washout in ethanol
Ormocer	Inorganic-organic hybrid	Use directly (Fraunhofer Institute Silicatforschung)	(1) Washout by 4-methyl-2-pentanone, (2) UV post-curing
PMMA	Methymethacrylate	Use directly (Microchem)	(1)Post-bake (2)wash out in Remover PG or Acryl strip

4 Resolution

Resolution of any optical instrument is its ability to clearly determine two separate points or objects. It is the least distance between the two objects that can be readily distinguished. The resolution of the lithographic system is characterized by the critical dimension (CD) which is given by:

$$\mathrm{CD} = \frac{k_f * \lambda}{\mathrm{NA}} \qquad (5)$$

According to the Equation 5 the critical dimension is directly proportional to the wavelength (λ) of exposure light and the proportionality factor (k_f) and inversely proportional to the numerical aperture (NA). In the last two decades these three quantities have been modified to decrease the critical dimension. The numerical aperture has increased from 0.5 to 1.35. This has been possible with the help of the liquid immersion objective. The space between the optical system and wafer in this objective is filled with transparent liquid of high refractive index. Decreasing the wavelength is another technique to decrease the critical dimension. Much progress has been made in 157 nm lithography. The proportionality factor k_f represents a combined effect of resolution enhancement technique such as a phase shifting mask, an off-axis illumination, improved photoresist quality etc. This factor has been reduced from 0.7 to 0.27. The combined modification of these parameters has led to a reduction in CD from 500 nm to 45 nm in time less than a decade. These are not the only parameters that affect resolution. There are other factors such as polarization effect, physical size of optics, photoinitiators cross section and so on [67]. In order to get detail insight of resolution let us start with point spread function (PSF).

4.1 Point spread function

The point spread function (PSF) of an optical system is defined as the irradiance distribution that results from a single point source. Let us consider a small object, say a 200 nm fluorescence bead. This bead can be considered as a point source of photon. This object is excited with a light source. The photons are guided to the camera with the help of the necessary optics and the microscope objective. Ideally, the image at the camera is thought to be a single point at the exact location of the bead. But the point spot is somewhat blurred or spread. In general this spreading which is the response of optical system to a point source of photon is considered as PSF. The two reasons for the point spread function are aberration and diffraction [68].

Let us assume $I_0(x,y)$ is the irradiation distribution on the object plane, an element dx dy located at (x,y) will radiant flux of $I_0(x,y)$ dx dy. This results into some sorts of blur spot over a finite area rather than point because of diffraction. The spread of the radiant flux is described mathematically by the function $\boldsymbol{\zeta}(x,y,X,Y)$ such that the flux density at the image point is given by:

$$dI_i(x,y) = \zeta(x,y,X,Y) I_0(x,y) dxdy \quad \ldots\ldots\ldots\ldots\ldots\ldots\ldots\ldots\ldots\ldots (6)$$

where, $\zeta(x,y,X,Y)$ is known as PSF. Consider the delta function is located at the point (x',y'). The quantity L{} is linear operator in the equation,

$$g(X,Y) = \iint_{-\infty}^{\infty} f(x',y') L\{\delta(x'-x)\delta(y'-y)\} dx' dy' \quad \ldots\ldots\ldots\ldots\ldots\ldots (7)$$

where f(x,y) and g(X,Y) being input and output of system. In a well corrected system ζ is the airy irradiation distribution function centered on the Gaussian image point [68]. In every lithographic or imaging system we need to consider 3D PSF. Figure 11 shows the point spread function at the focus in the transverse plane at z = 0 (left) and axial plane at y = 0 (right)

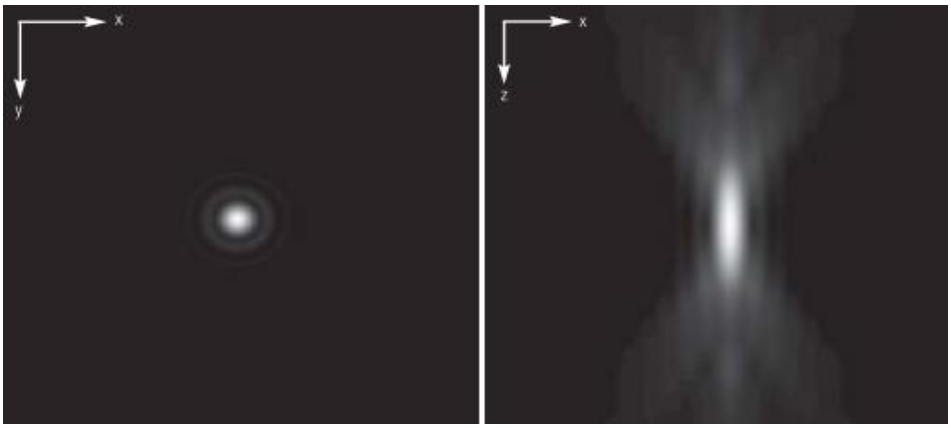

Figure 11: Intensity distribution of the PSF at the focus in the transverse plane at z = 0 (left) and axial plane at y = 0 (right). [69].

4.2 Lateral and axial resolution

In any optical instrument like a telescope and a microscope, resolution is the ability to distinguish two nearby sources in 3D. Consider two point sources that lie on the same plane of focus. These points are moved closer to each other and consequently they are not seen as two separate points. The smallest distance at which they are seen as two different points defines resolution. As mentioned earlier the resolution should be viewed three dimensionally.

Resolution in xy-plane is known as the lateral resolution and is defined as the smallest distance between the two points at which they can be viewed as separate objects in xy-plane. The lateral resolution is given by the following equation:

$$\mathrm{FWHM}_{\mathrm{lateral}} = \frac{0.51 * \lambda}{\mathrm{NA}} \quad \ldots\ldots\ldots\ldots\ldots\ldots\ldots\ldots\ldots\ldots\ldots\ldots\ldots (8)$$

where, NA is the numerical aperture of microscope objective and λ is the excitation wavelength [69].

Similarly the axial resolution is defined in xz-plane. By analogy with lateral resolution, it is defined as the smallest distance between separate object that can be distinguished clearly in the z direction. The axial resolution is given by the following equation:

$$\mathrm{FWHM}_{\mathrm{axial}} = \frac{0.88*\lambda}{(n-\sqrt{(n^2-NA^2)}}\ldots\ldots\ldots\ldots\ldots\ldots(9)$$

where, NA is the numerical aperture of the microscope objective and λ is the excitation wavelength [69].

4.3 Resolution in two-photon polymerization

Resolution in case of two-photon polymerization is the smallest achievable feature characterized by the volumetric pixel (voxel). Voxel is the solidified resin at the focal spot. The shape of the voxel coincides with the grain of rice. The width and height of the voxel determines the photopolymerisation resolution. In order to achieve an optimal resolution the power and exposure time should be well optimized. The resolution of two-photon polymerization can go below one micron. In order to maximize the resolution, the focusing optics should be well adjusted. It is recommended to use high magnification objective with a high numerical aperture. Apart from laser optics, the laser dose contributes to the size of the voxel. This optical laser dose is the product of the exposure time and the power of the laser. The resolution is high when the power is low (above the polymerization threshold) and the exposure time is short [70,71].

Figure 12 shows the excitation efficiency of a single-photon polymerization (1PP) and two-photon polymerization (TPP). The wavelength of light used for 1PP and TPP are 375 nm and 750 nm respectively. The numerical aperture is 0.75 for both cases. As seen from the figure, the FWHM is bigger for two-photon polymerization than single-photon polymerization. The reason of the small FWHM for 1PP is due to smaller wavelength of light used than TPP. As calculated from the Equation 8, the FWHM for TPP is 510 nm but the figure 12 shows that the FWHM is decreased to 360 nm. This is because of the non-linearity of two-photon excitation. The excitation rate decreases quadratically as the distance from the focal plane (z) increases in case of TPP. This is not the case with 1PP where the excitation rate decreases linearly as the distance from focal plane increases.

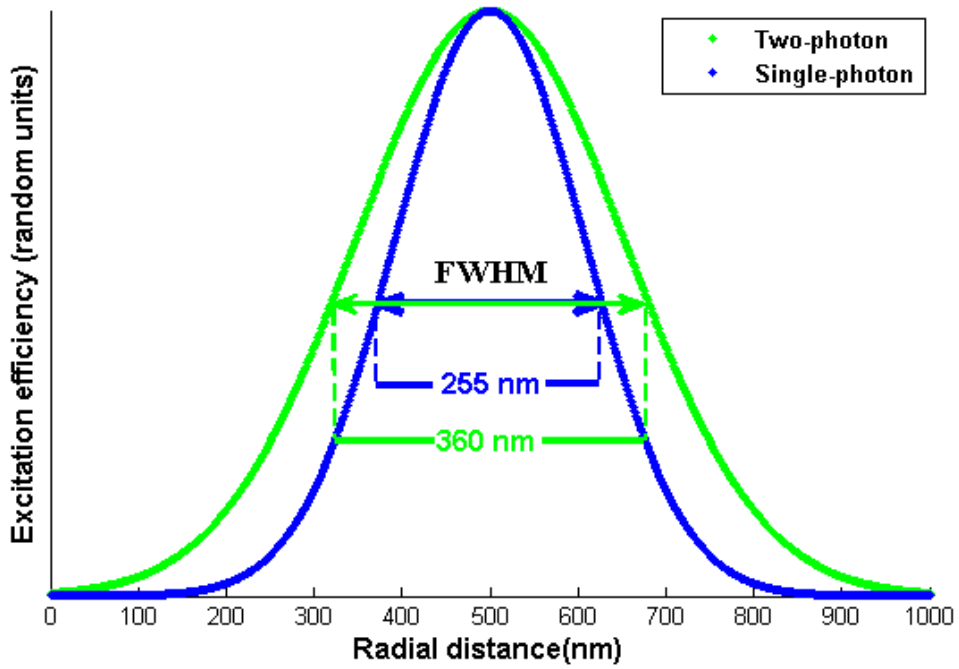

Figure 12: Profiles of excitation efficiency showing FWHM for 1PP (375 nm) and TPP (750 nm).

4.4 Mathematical model to calculate resolution

The mathematical model [72] for the calculation of the voxel size is explained in this section. The resolution beyond the diffraction limit can be achieved by controlling the laser pulse energy and the exposure time. We can calculate the size of voxel by defining the polymerization threshold. Let us assume the resin is polymerized as the radical density $\rho = \rho(r,z,t)$ exceeds a certain threshold $\rho_{th.}$ The intensity distribution of the laser beam is rotationally symmetrical. Hence ρ can be expressed as the function of z, r and t. Here z is distance to the focal plane in cylindrical coordinates, r is distance to the optical axis in cylindrical coordinates and t is the total processing irradiation time.

The radical density $\rho(r,z,t)$ produced by the femtosecond laser pulses can be calculated by solving the rate equation given by;

$$\frac{d\rho}{dt} = (\rho_o - \rho)\sigma_o N^2 \,, \quad \text{.....(10)}$$

$$\text{and } \sigma_2 = \sigma_2^a \, \eta \text{.....(11)}$$

In the above equation σ_2 is symbol used for the two photon cross section for the radical generation, σ_2^a is the ordinary two-photon absorption cross section and η is efficiency of initiation process which is always less than unity. Let us consider the photon flux be N=N(r, z, t), ρ_o is the primary initiator particle density. The approximation of the light distribution in the main maxima at the focal plane (z=0) is done with the aid of the following Gaussian distribution formula.

$$N(r,t) = N_o(t)\exp\left(\frac{-2r^2}{{r_o}^2}\right) \text{.....(12)}$$

Here $N_o(t) = N_o$ is the photon flux on the optical axis which is considered to be constant.

We neglect the losses of the radicals between the laser pulse and can estimate the voxel diameter (d) as,

$$d(N_o, t) = r_0 \left[\ln\left(\frac{\sigma_2 N_0^2 \tau_L}{C}\right)\right]^{1/2} \quad \text{.....(13)}$$

Here the symbol $\eta = \upsilon t$ is the number of pulse, υ is laser pulse repetition rate, t is total time processing irradiation time and τ_L Here *C* is defined by

$$C = \ln[\rho_0(\rho_0 - \rho_{th})] \quad \text{.....(14)}$$

The estimation of the maximum voxel length along the beam axis at r=0 can be done by using the expression for the axial light distribution.

$$N(z) = N_o\left(1 + \frac{z^2}{z_R^2}\right) \quad \text{.....(15)}$$

Here z_R is Rayleigh length.

Thus the voxel length is calculated by

$$l(N_o, t) = 2z_R\left[\left(\frac{\sigma_2 N_0^2 \eta \tau_L}{C}\right)^{\frac{1}{2}} - 1\right]^{1/2} \quad \text{.....(16)}$$

From the equations 16 and 13 above, we can calculate the length and diameter of polymerized voxel.

Here for calculating the resolution N_o can be replaced by

$$N_o = \left(\frac{2P\ \varphi}{\pi r_0^2 \tau_L\ \upsilon \hbar \omega_L}\right) \quad \text{.....(17)}$$

Here P is the average laser power, ω_L is the frequency of the laser used, and φ is the fraction light transmitted through objective.

4.5 Resolution enhancement technique

The development of the liquid immersion objectives with high numerical aperture and decrement of the wavelength of the light used are the fundamental aspects of resolution enhancement. Now, the concept of Stimulated emission depletion (STED) is also emerging as a strong tool for resolution enhancement in optical lithography. The STED concept provides a straightforward way to overcome the diffraction barrier. No doubt the concept of STED formulated by Stefan Hell is a breakthrough in breaking the diffraction barrier in optical microscopy. The stimulated emission deactivation beam used in the photopolymerisation lithography is thought to enhance the resolution down to 10 nm. The achievement of 10 nm resolution in x, y, z directions is a nano-technologist dream come true which would be another breakthrough in the field of lithography [73,74].

The two beams, excitation beam and de-excitation beam, are used to excite molecule and de-excite back to ground state respectively. The de-excitation beam, also known as STED-beam, is usually doughnut-shaped beam. The main role of this STED-beam is to decrease the spontaneous emission by increasing the stimulated emission. In

theory, the resolution is limit free in STED microscopy. The removal of the microscopy and insertion of the lithography in STED is not easy task. The main challenge is to develop of the suitable resist material [74].

Figure 13 shows the schematic Jablonski diagram of photoinitiator molecule based on radical polymerization. By the process of two-photon absorption the molecules are excited to electronically excited level which is followed by non-radiative transition. The excited molecules go to triplet state by intersystem crossing in the time scale of the order of 100 picoseconds. The radicals that lead to photopolymerisation are formed at triplet state. The main idea of this technique is to de-excite the molecule before the intersystem crossing [3,74].

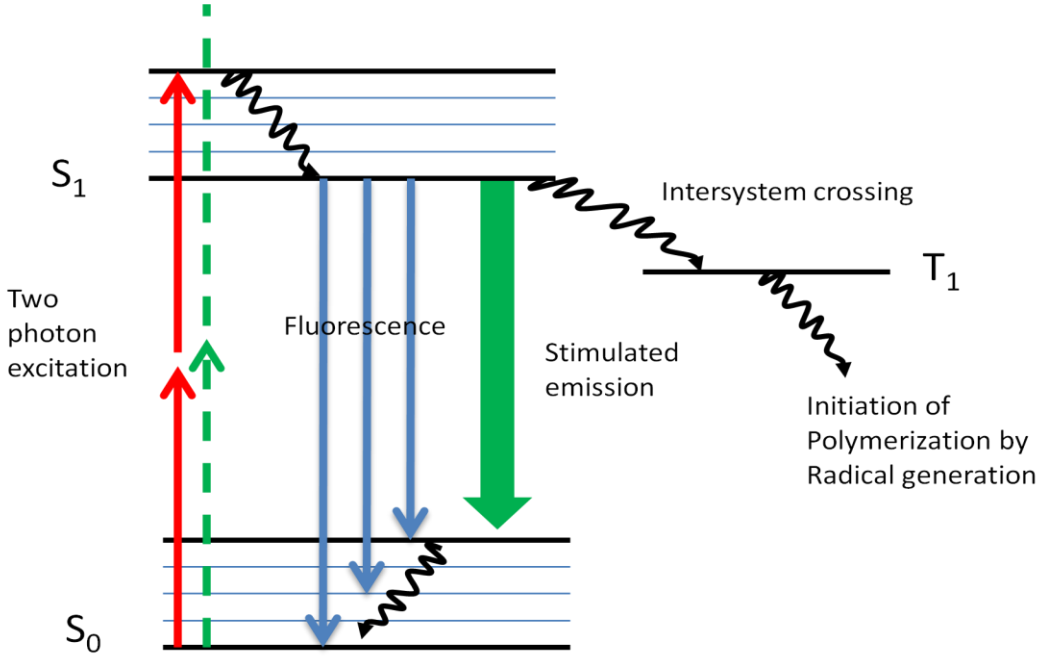

Figure 13: Schematic Jablonski diagram of photoinitiator molecule and its optical transition and process [74].

To implement the concept of this STED-photopolymerisation, the oscillatory strength of molecules between the ground and the first excited state has to be large. If so, the stimulated emission dominates absorption from first excited state to higher excited state. However the oscillator strength of many photoinitiator molecules is small. In this case, the de-excitation beam enhances polymerization due to the two-photon absorption of the de-excitation beam and degrades the resolution. This is a big challenge to implement the STED on polymerization. The solution is to search the photoinitiator molecule with larger absorption cross section than typical radical photoinitiators. The focus of search should be on the molecule with high fluorescence quantum yield [3,74]

The resolution in case of two-photon polymerization can also be enhanced using Diffractive Super Resolution Element (DSE). In this technique we employ the two-photon polymerization theory and optical diffraction theory. The Diffractive super resolution element rearranges the Point spread function of the focus. DSE is introduced

before the objective lens. In the Figure 14, dotted line segment is the shape of the concentration of radical before placing DSE and solid line segment represents the concentration of radical after placing DSE. The FWHM is greater for dotted line than solid line. Thus the curve shows that there is enhancement of resolution while using DSE [75].

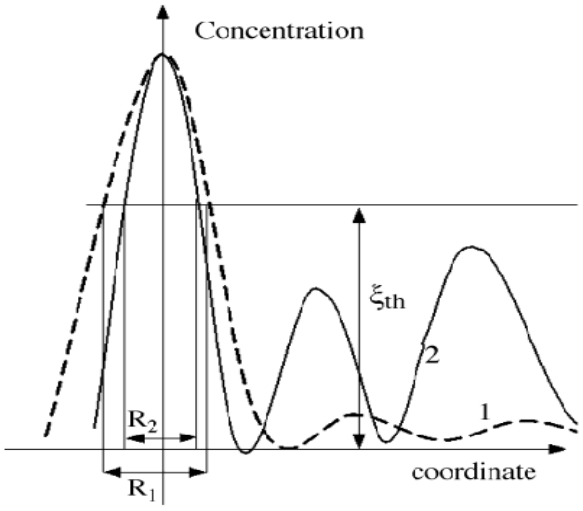

Figure 14: Schematic representation of shape of the concentration of radical before placing DSE(dotted line) and solid line segment represents the concentration of radical after placing DSE (solid line) [75]

5 Methodology

This chapter deals with the methods of performing experiments in laboratory. The custom built TPP setup is described in detail below. The process of sample preparation and implementation of scanning are illustrated. The method of resolution calculation and the fabrication of the 2D structure are also explained below.

5.1 Calibration

The camera used in this work was a CMOS DCx USB camera. The size of the single pixel in the imaging plane of this camera was measured and used for distance measurement. The calibration was done with a 75 µm pin-hole. At first the pin-hole was mounted on the sample stage, magnified by the objective and imaged by the camera. The diameter in term of pixel was calculated which corresponds to the diameter of the pinhole (75 µm). Now the length in the imaging plane corresponding to single pixel of camera was calculated. This value was fed into uc480 viewer software (application software for operating camera) as a measurement unit. After this the distance of the fabricated structures were measured in terms of micrometer unit.

The stage used was NanoMax TS 3-axis flexure stage which was calibrated against MDT693 Piezo controller manufactured by Thorlabs and National Instrument (NI) 6363 DAQx card. The MDT693 Piezo controller operates only in the open loop mode. This controller was replaced by a BPC203 Piezo controller manufactured by Thorlabs. This controller can be used in the both open and closed loop mode.

5.2 Optical setup

A custom-built two-photon photopolymerisation setup was used to demonstrate proof-of-principle nanofabrication. Here, we used a diode laser pumped Titanium-Sapphire (TiSa) femtosecond laser as an excitation source. This is a tunable laser which can be tuned from 650 nm to 1100 nm. This laser has the ability of emitting ultra short femtosecond pulses. The TiSa laser uses the sapphire crystal (AL_2O_3) doped with the titanium ions as the gain medium. The pulse repetition rate of the laser was around 80-100 MHz and the pulse width was roughly below 150 fs. In all experiment the average power used in front of the objective lens ranged from 35-60 mW. We tuned the operating power of TiSa laser to 745 nm to optimize the output from acousto-optical modulator (AOM). The laser power was controlled by the polarizer located in front of the AOM. Figure 15 shows the optical setup for nanofabrication using two-photon polymerization.

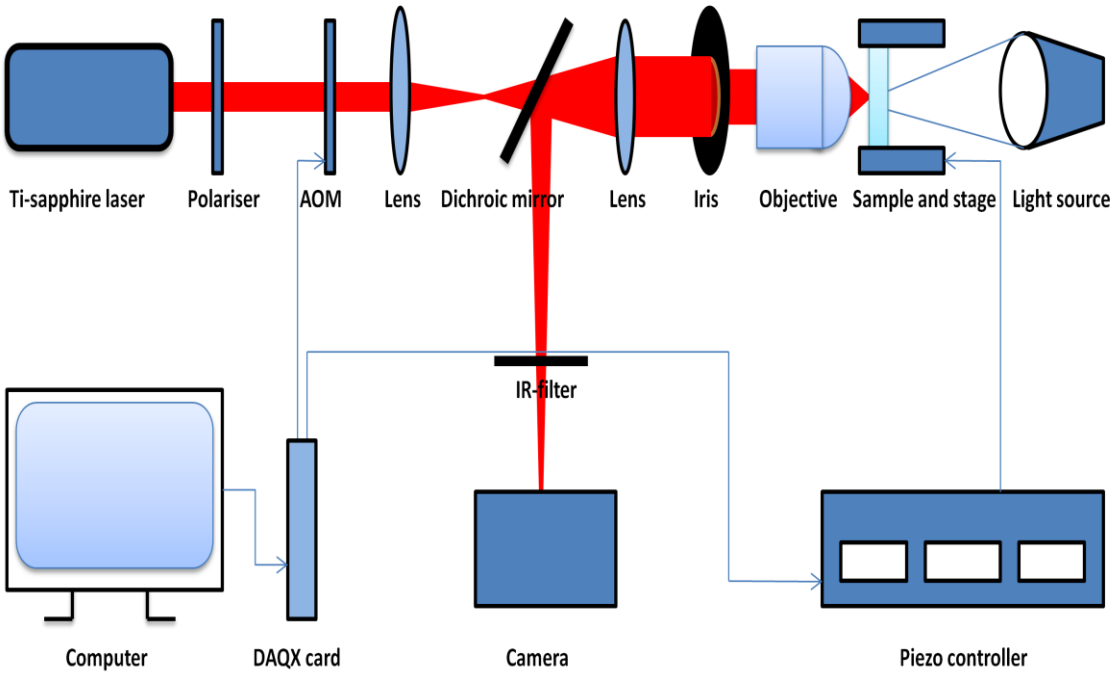

Figure 15: Instrumental setup for nanofabrication using two-photon polymerization implementing vectorial writing.

The AOM was used as a shutter in the setup. With the aid of the sound wave, AOM (Acousto-optic modulator) diffracts the light. This device is also known as the Bragg cell. In principle, the light beam coming from the laser source interacts with the sound wave inside the AOM. With the interaction of the laser beam and the sound wave, the light beam is forced to diffract. Thus the light is diffracted in the presence of the sound wave and is not diffracted in its absence [76]. The zero order beam was used to write the desired structure when the AOM was closed. A certain amount of light was reduced from the zero order beam when the AOM was operating. Thus decreasing a certain amount of light from the zero order beam decreased the power below the polymerization threshold; hence the writing process did not take place. The collimator, a combination of two lenses, was used to increase the beam diameter. The 40 mm and 200 mm Plano-convex lenses were used. This assembly increased the beam diameter by 5 times the original diameter.

The expanded beam was then directed to an infinity-corrected objective lens (50 X, 0.75 NA Leica). This objective focused the laser beam into the photoresist mounted on a 3-axis motorized stage (Nanomax, Thorlabs). This stage facilitated scanning in the TPP setup with internal piezo actuator which not only held the sample but also moved in x, y and z directions for three dimensional writing. The stage could move a maximum of 4 mm and had a strain gauge displacement sensor which provided an analog signal proportional to the displacement with a resolution better than 5 nm. The piezo electric actuator, built inside the stage, provided the range of 20 µm displacement. The stage was used in both closed loop mode and open loop mode. Hence in the experiment both the open loop and closed loop modes were implemented to fabricate structures.

The piezo controller used was Thorlab's BPC203 piezo controller which was used to control the movement of nano max according to our need. The DAQx card was used to input analog signal to the piezo controller via BNC cables. This piezo controller was APT system multichannel piezo controller. This could be used in both open and closed loop mode. This controller was controlled manually as well as by computer using APT software. The National Instrument 6363 model DAQx card used in this setup had four output channels. They were used to supply external voltage to three piezo channel so that it controls the movement of the stage in all the three directions. One of four output channels of the DAQx card was programmed via Labview in order to control the operation of AOM.

A dichroic mirror, a specialized mirror that transmits the near infrared (NIR) and reflects visible (VIS) light, was inserted in the excitation path at 45°. This directed the scattered signal from the resin plane towards CMOS camera (DCx USB Camera, Thorlabs) for real-time visualization of the photopolymerisation process. A white light source situated on the transmissive side of the objective was used to illuminate the resin. The image formed at the CMOS camera was viewed via computer.

5.3 Scanning system

Two kinds of scanning can be applied in our setup. They are raster and vector scanning. In the case of raster scanning the laser beam focus is moved through each pixel. The shutter is opened for the certain value of pixel above threshold according to our need else closed. This type of scanning is relatively slower than vector scanning as the laser pointer has to scan through large number of sample points (pixels). As our DAQx card had a limitation of 9000 sample points, this kind of scanning was avoided. And there was another disadvantage too. The fabricated area using raster scanning has extra shape which scatters the light while polymerizing the resin. This is due to the fact that the polymerized area in the first line solidified before scanning the second line. This solid polymerized area scatters the light while polymerizing the second line. Hence raster scanning was not used even in this work.

In vector scanning each pixel is not scanned but the neighboring pixel with the desired intensity is checked. At first, the arbitrary pixel value is addressed in the scanning area. The pointer is moved to the next pixel if the pixel has correct intensity. This process continues until the pointer scans the whole specified area. The shutter is open throughout scanning. Here the Freeman algorithm was employed which followed the vector scanning so that we could draw any arbitrary structure that we wanted. Freeman algorithm commonly known as Freeman chain code algorithm is an image processing algorithm where the outer edge of the image is followed by the laser beam (pointer) in a certain direction in order to write a structure. Before applying the chain code the numbers of sample points were reduced by sub sampling process. Figure 16

represent the schematic view of Freeman contour of map of Finland. The outline or contour of the images was not branched or discontinuous at any pixel which was a necessary condition for Freeman chain code algorithm.

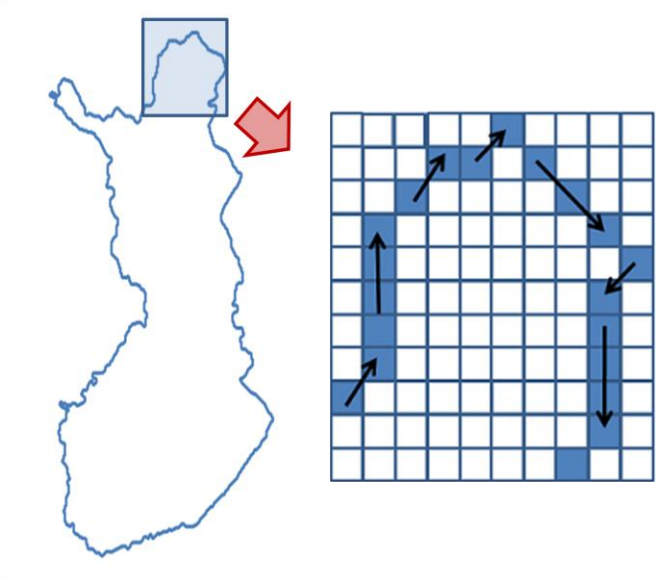

Figure 16: Schematic presentation of Freeman contours of map of Finland.

A schematic view of raster scanning for writing alphabet E is shown on the Figure 17 (left). The laser pointer traverses through the each pixel starting from the first pixel of first row to last pixel of last row one by one. The shutter is closed for a hollow circle and is opened for a solid circle. Figure 17 (right) depicts the vectorial scanning method. Here, the laser pointer moves only through the solid circle in a certain direction as specified by the line arrow. Here the shutter is open throughout the scanning.

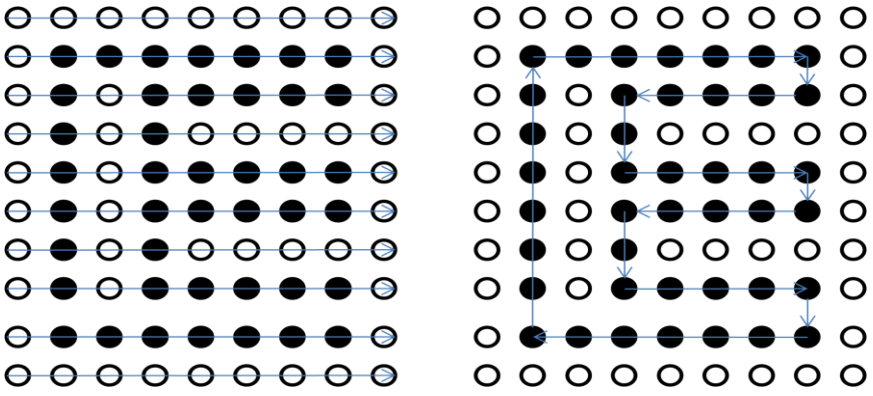

Figure 17: Illustration of raster (left) and Vector (right) scanning.

5.4 Sample processing

In this thesis work, the samples were prepared in clean room located at the Department of Bio-measurement of Tampere University of Technology (TUT). The exposure procedure was performed at the Optics laboratory of the Department of Physics of TUT. Finally the structures were imaged at the Optoelectronic Research Center (ORC) located at TUT.

The sample processing started with the cleaning of the glass substrate. The substrate used in this experiment was 25 mm diameter micro-cover glass manufactured by Electron Microscopy Group. The cleaning process consisted of a couple of the steps; wiping with acetone, treatment with Piranha solution and RIE **(**Advanced Vacuum Vision 320 Mk II RIE**)** cleaning. The cleaning process began with cleaning the glass wafers with acetone. The glass wafers were wiped with acetone and clean room paper. The particles detached from the wafer were removed via air gun. After cleaning with acetone, the process was followed by Piranha treatment. In the case of Piranha solution treatment, 20 ml of sulfuric acid was poured into decanter and it was set onto the hot plate at 80 degree Celsius. The wafers were carefully placed into the decanter and 15 ml of hydrogen peroxide was added. The solution was then heated for 20 minutes. The Piranha treatment was followed by RIE cleaning.

The two hot plates were set to 65^{o}C and 95^{o}C. The cleaned glass cover slip was kept in the spin coater (Laurell WS-400) in such a way that the wafer stays exactly onto the center of holder. The wafer was checked by spinning the holder if it was on the centre or not. The vacuum was used to attach the wafer to the holder. The spin coating speed was chosen according to the data sheet provided by Microchem. The SU-8 5 was poured onto the centre of the glass wafer. To prevent an air bubble the mouth of the SU-8 bottle was kept as near as possible to glass wafer. After pouring the SU-8 the mouth of the SU-8 bottle was wiped with acetone so that no curing occurs in the mouth of bottle. The spin coating program was set according to the data sheet provided by the Microchem (the data sheet provided by microchem is mentioned in reference [59]). After the completion of the spinning program, the lid of the spin coater was lifted carefully so that the droplets of the SU-8 don't drop on the sample.

The wafer was placed onto the middle of the hotplate temperature set at 65^{o}C. This was baked for 1 minute. After this was done, the sample was transferred to the other hot plate at 95^{o}C for 3 minutes. This change in the temperature from 65^{o}C to 95^{o}C was done in order to avoid a quick temperature jump. The sample was kept level on the hotplate in order to gain the planar SU-8 surface. After completion of baking, the sample was ready for the exposure.

The sample was brought to the laboratory where we had the TiSa laser with the necessary optical instrumentation. The sample was exposed to fabricate the different structures as needed. Care was given that the ambient light doesn't expose the sample so that sample cures before exposing with the laser. With the necessary condition checked

in the datasheet provided by the Microchem, the post-exposure bake was performed. Again to avoid the temperature jump the sample was baked for the 1 minute at 65^{o} C and for 1 minute at 95^{o} Celsius.

The developer (Mr-Dev 600) was poured in a clean decanter. The glass wafer was immersed into the decanter and shaken every once in a while. Though the development time was mentioned 1 minute in the Microchem data sheet but it was necessary to develop the resist longer than the time given in the data sheet. When the mold was developed for enough time it was washed with the Isopropanol. While washing with Isopropanol, if white color appeared in the sample, it was further developed. Finally the mold was rinsed with the distilled water and dried with the nitrogen gun.

The imaging system in the fabrication setup with 50 X Leica objectives was used for the pre-development and the post-development imaging. The pre-development imaging was done in order to ensure if the polymerization was taking place or not. The post-development imaging was employed in order to ensure that the fabricated structures were correctly developed or washed away. For the detail and precise imaging, the scanning electron microscope (SEM) was used. The sample was sputtered with gold nano-particles to a thickness of 10 nm and imaged by SEM.

5.5 Determination of resolution

Resolution in TPP can be calculated using two methods, either by using array of voxel or by drawing simple lines. In the case of the voxel array method, individual voxels are created by shooting a laser light into the sample for few milliseconds. After the resist is exposed for the desired amount of time the sample is moved to new position and the exposure is repeated again. This process is repeated again and again in order to create hundreds of voxel. Figure 18 represents the lateral and axial diameters of a voxel. During resolution calculations these two diameters are measured. In order to do so the height of the voxel should be adjusted. Position b is the correctly adjusted voxel for the lateral resolution calculation. Positions d and e are correctly adjusted height for axial resolution calculation.

The voxel array method was not employed in this thesis for calculation of resolution. The problem with this method is unavailability of whole dots. Many of them get washed completely or partly. Hence the line array method was employed in this thesis to study resolution.

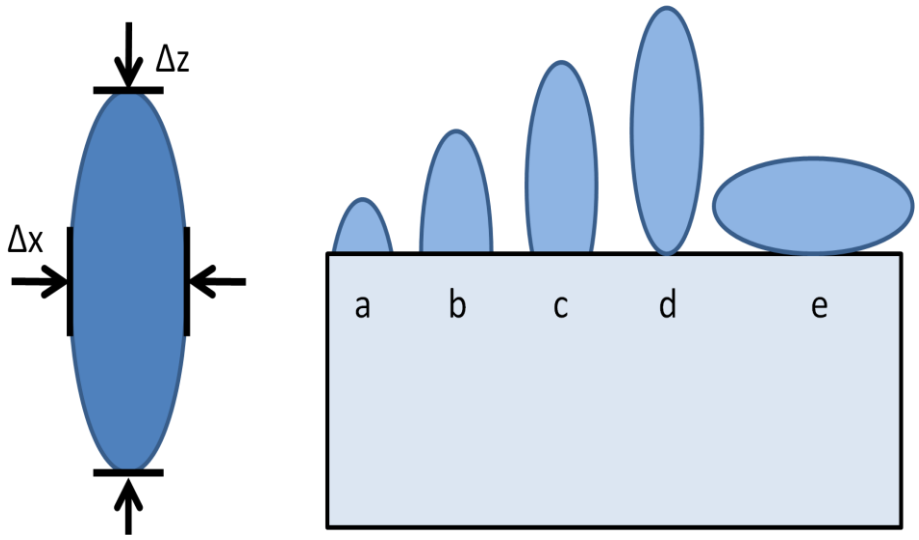

Figure 18 : Shape of single voxel (left) representing lateral and axial diameters of a voxel. Voxel position for measuring lateral and axial diameters (right). Position b is correct position for lateral diameter calculation while positions d and e are correct positions of voxel to measure the axial diameter of voxel.

Resolution can also be calculated by drawing series of two dimensional lines in photo resist. This series of two dimensional lines are drawn with different laser power and scanning speed. The scanning speed is directly related to exposure time; hence scanning speed shows significant effect on the resolution. Usually the scanning speed and the laser power are optimized before drawing a series of line for resolution calculation. The width of the line determines the x-y direction resolution and height of line determines the z direction resolution. The width of line can be measured by employing SEM with the electron gun focusing at 90º. It is a bit difficult to measure the height of the line. Either the gun has been tilted in order to measure the height of the line or the sample should be cut vertically near to the line. The simple approach is to measure the fallen line with employing the electron gun at 90º.

5.6 Fabrication of two-dimensional structure

At first the simple picture of structure was processed by using MS-Paint (Windows). The processing of a picture was done to ensure that the necessary conditions were fulfilled for the Freeman code generation. The Freeman algorithm was written in Matlab which generates the Freeman codes. The Freeman code was fed into Labview program. It was programmed to tailor the output of the DAQx card in order to control the movement of stage in x, y and z directions. The fabrication was done in such a way that the laser beam remains at fixed position and the stage moves the sample in 3D planes so as to fabricate the complex structure. All the structures presented here were fabricated employing closed loop piezo controller except the arrays of straight line.

6 Result and discussion

After the completion of the building custom built TPP setup, series of experiments were performed. The results are presented and their cause and consequences are discussed below. At first the outcome of the calibration of the CMOS camera and Nanomax stage are presented which is followed by the results of optimization of different polymerization parameter. The resolution is calculated and image of different fabricated structures are presented. At last, the aspect ratios of the different fabricated lines are tabulated. These results are discussed below in detail.

6.1 Calibration

The diameter of pinhole in term of pixel was found to be 726 pixels. This means 726 pixels corresponds to 75 µm (diameter of pinhole). Thus the size of the single pixel corresponds to 0.103 µm. The Nanomax stage is moved by 20 µm (maximum) with 75V. MDT693 piezo controller amplifies the voltage by factor 15. This means the maximum voltage that can be applied from DAQx card is 5V. Thus 5V signal from DAQx card moves the Nanomax stage by 20 µm. But the BPC203 piezo controller in closed loop mode amplifies the voltage by factor 7.5 which signifies that a 10V signal is required to move the stage 20 µm.

6.2 Selection of photoresist

There were many commercially available photoresists with plenty of option for the selection. The SU-8, 5 photoresist with viscosity 290 cSt was selected for this study. This viscosity value permits the resist thickness of 5 µm at minimum. The selection procedure of photoresist started with checking the wavelength range of the Ti sapphire laser source. This laser can be tuned from 650 nm to 1100 nm. The absorption spectra of this photoresist showed the spectra starting from 370 nm. This resist can be conventionally processed from the 350 nm to 400 nm. As we were more concerned about two-photon polymerization the resist can be irradiated with 700-800 nm radiation. This was the range of wavelength where the laser works best.

The properties like matching refractive index, high aspect ratio and wide popularity were also the reason for the selection of this SU-8 resist. Though the SU-8 has poor adhesion capability with the substrate, but this draw back was overcome by using the Piranha solution treatment. There were varieties of the SU-8 resist available at

market manufactured by Microchem namely SU-8 2, SU-8 5, SU-8 10, SU-8 25, SU-8 50, SU-8 100, SU-8 2000, SU-8 2100 etc. These variety of photoresist differ on their viscosity property and consequently on the thickness of resist. Among these varieties SU-8 5 was selected for our fabrication. Using this resist, we could spin coat a layer of smaller thickness over a substrate. This was the reason for selection of SU-8 5. Tests were also made using SU-8 50 and SU-8 100. The minimum thickness that these resists offer was 40 µm. The fabrication was difficult to perform as it requires more power. There was no polymerization below 70 mW using these two samples. So the conclusion was made to use the photoresist with low viscosity. The SU-8 5 was finally selected and the resist with 15, 7 and 5 µm thickness layer were coated onto the substrate.

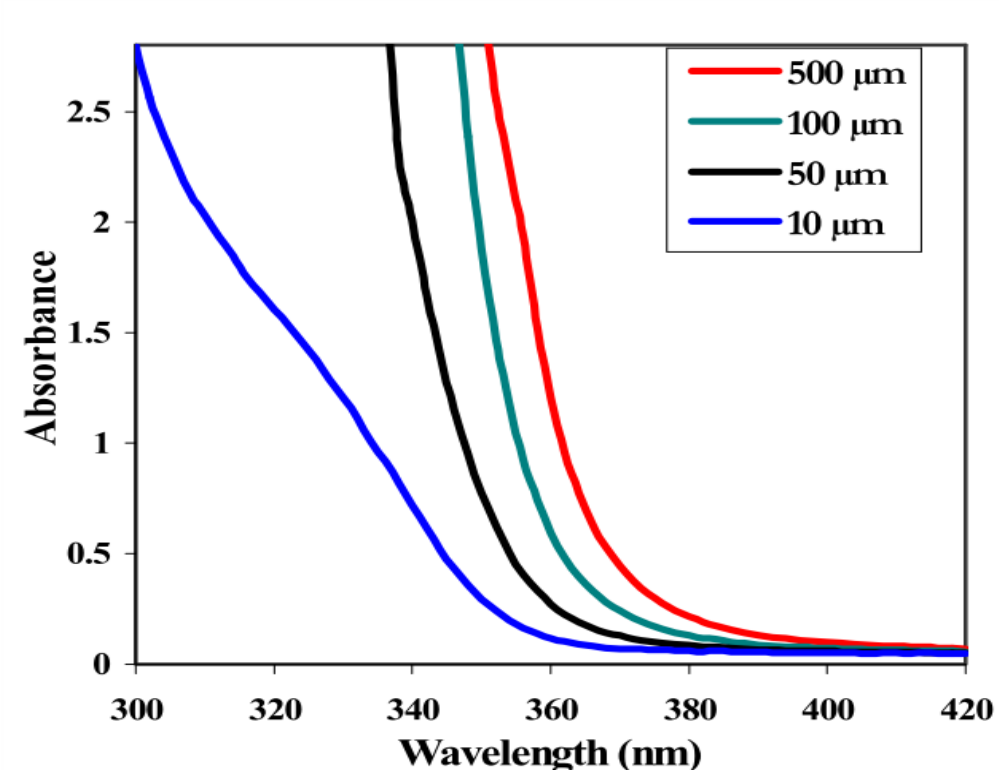

Figure 19: Absorption spectra of SU-8 photoresist of different film thicknesses. The absorption spectra above showed the absorbance starting from 370 nm which means the resist can be conventionally processed from the 350 nm to 400 nm [59].

6.3 Optimization of photopolymerisation parameters

At first the photoresist quality was optimized. The selected photo resist was checked for quality. The two parameters, adhesive property and development time was checked for quality of the photoresist. At first the SU-8 photoresist was spin coated onto the substrate which was only cleaned with acetone. This was exposed with the laser beam of different power and scanning speed. After this the irradiated sample was developed

by Mr. DEV 600 developer. The developed sample was imaged using the visible light imaging arm of the TPP setup. The result after imaging showed almost no structures. Later this was confirmed by SEM imaging. The reason behind this was difference in electrical polarity. SU-8 is polar material while the glass is non-polar hence the adhesion probability of this photoresist is restricted to few percent. This kind of poor adhesion usually results in structural failure and low aspect ratio with low survival rate after development.

Now the substrate was cleaned by acetone followed by Piranha treatment. The Piranha solution used in this case was H_2SO_4 (20 ml) and H_2O_2 (15 ml). The substrate was boiled in Piranha at 80^oC for 20 minutes. The spin coating and exposure procedure were repeated. After development, the imaging system showed significant improvement in the result. This was again confirmed by SEM. This means that the adhesion capability of the SU-8 was increased by the Piranha treatment. The reason was quite obvious. The non polar glass substrate is changed into polar by the Piranha treatment. H^+ ions are coated on the surface by the acid treatment. These H+ moieties make the glass polar which facilitates adhesion [63].

In the third experimental procedure, the substrate was cleaned with acetone, treated with Piranha, and is further cleaned with RIE (Reactive Ion Etching). As before, necessary experiments were done and finally imaged by SEM. The result didn't show significant improvement over the second experiment performed. Though the use of RIE is recommended for substrate cleaning but this cleaning was discarded as it was much more time consuming.

The development time was also optimized. The resist was allowed to develop for certain period of time as mentioned in data sheet provided by Microchem. After this development time, the sample was cleaned with Isopropanol. There was the white matter seen in the sample which means that the development time was not enough. Now for the next resist the development time was increased and washed with Isopropanol and this process was repeated until the sample is fully developed. This development time was around 25 % more than the mentioned development time in datasheet. After this experiment, the development time was increased by 25 % for every development.

After optimizing the photoresist quality, the thickness parameter was optimized. The thickness of the resist layer depends on the spinning speed and the viscosity of the resist. Here, three resist thicknesses were considered. They were 15 µm, 7 µm and 5 µm. In order to achieve the thickness of 15 µm, 7 µm and 5 µm, the spinning speeds were set to 1000 rev/min, 2000 rev/min and 3000 rev/min respectively. At first the 15 µm thickness resist layer was irradiated with the laser beam of different power and scanning speed. The polymerization threshold was around 52 mW which means that the polymerization only takes place above 52 mW. The line widths of fabricated lines were above 1 µm. The results were not satisfactory so the next sample with thickness 7 µm was irradiated. Here the lines with width 400 nm to 1000 nm were fabricated. Almost similar results were found with 5 µm thickness resist. The threshold for 7 µm and 5 µm

thickness resist were around 42 mW and 40 mW respectively. The result showed that there is significant decrease of line width with decrease of the thickness of photoresist layer. The threshold also decreases with the decreasing thickness. Figure 20 illustrate the results obtained in optimizing thickness parameter.

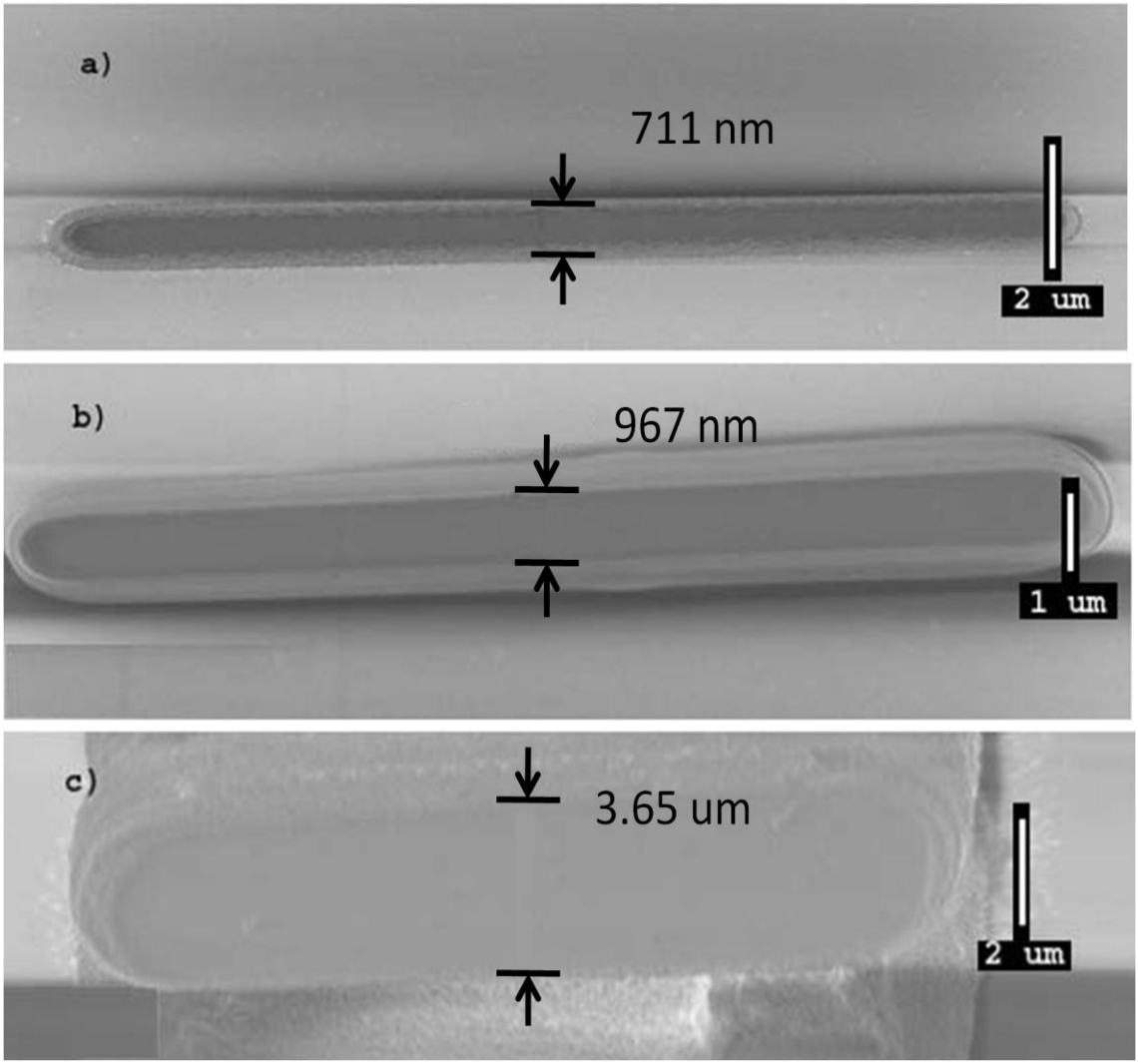

Figure 20: Optimization of thickness parameter a) line of width 711 nm drawn at 5 µm thickness b) line of width 967 nm drawn at 7 µm and c) line of width 3.65 µm drawn at 15 µm.

After optimizing thickness, laser power was optimized. In this experiment, the laser beam with different powers was irradiated onto the sample at a constant speed (constant exposure time). The laser power could be varied using pumping power but this was avoided as the pumping was quite sensitive. The pump power was kept constant well above the threshold. The laser power was controlled by the polarizer located in front of the AOM. The thickness of the sample considered was 5 µm. The power was set to 55 mW and is gradually decreased by 3 mW till the power threshold was reached. The scanning speed was kept constant. Keeping the scanning speed constant the width of line is plotted against the laser power which is shown in Fig 21. The graph shows that

there are no lines drawn below the threshold power below 40 mW. Above the threshold power, photopolymerisation is initiated. As we increase the power, the width of the line increases gradually and saturates. If we further increase the power micro boiling occurs due to excess radiation. The reason is quite obvious. There is no formation of initiating species that initiates polymerization below threshold. As we increase the power above the threshold there is a formation of radical species which initiates polymerization reaction. Then the photo initiators are excited to higher energy level. A further small increase in power leads the larger number of photo initiators to higher energy levels and finally reaches saturation such that there is no further increase in line width.

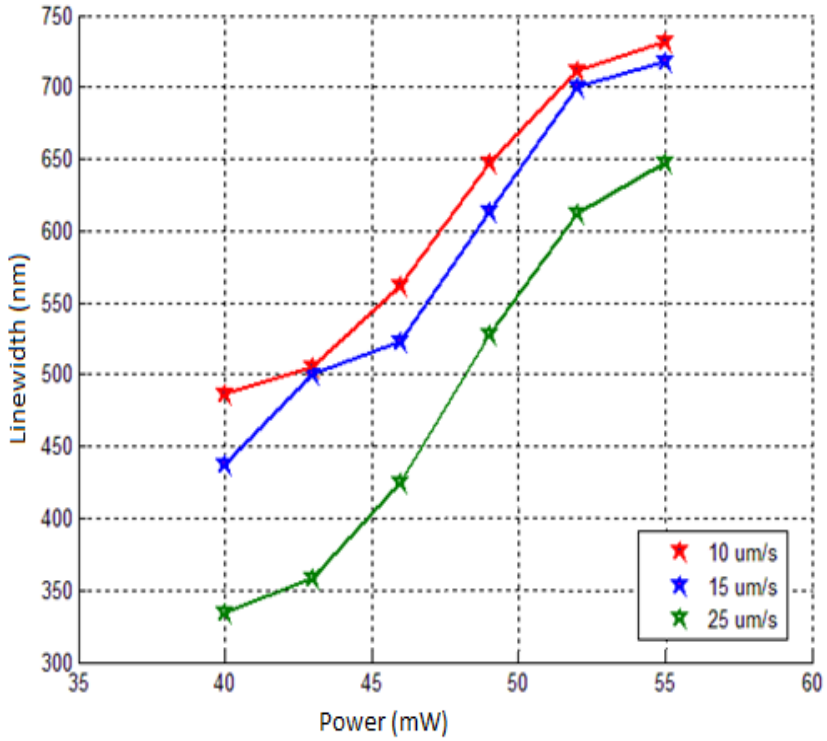

Figure 21: Variation of fabricate line widths with incident laser power at constant scanning speeds of 10 um/s, 15 um/s and 25 um/s.

For scanning speed optimization, multiples lines were drawn at constant power with varying scanning speed. The scanning speed is directly related to exposure time. Here, the thickness of the sample considered was 5 µm. The power was set constant and the scanning speeds were varied from 1 µm/s to 25µm/s. The width of the line was plotted against the scanning speed at constant power. Figure 22 shows that when the scanning speed is low, the line width is at constant because the excited photo initiators are at saturation as the exposure time is high. As we go on, increasing the scanning speed, the line width starts to decrease and at a certain point below threshold, there is no polymerization. This reason coincides with the explanation for Figure 21.

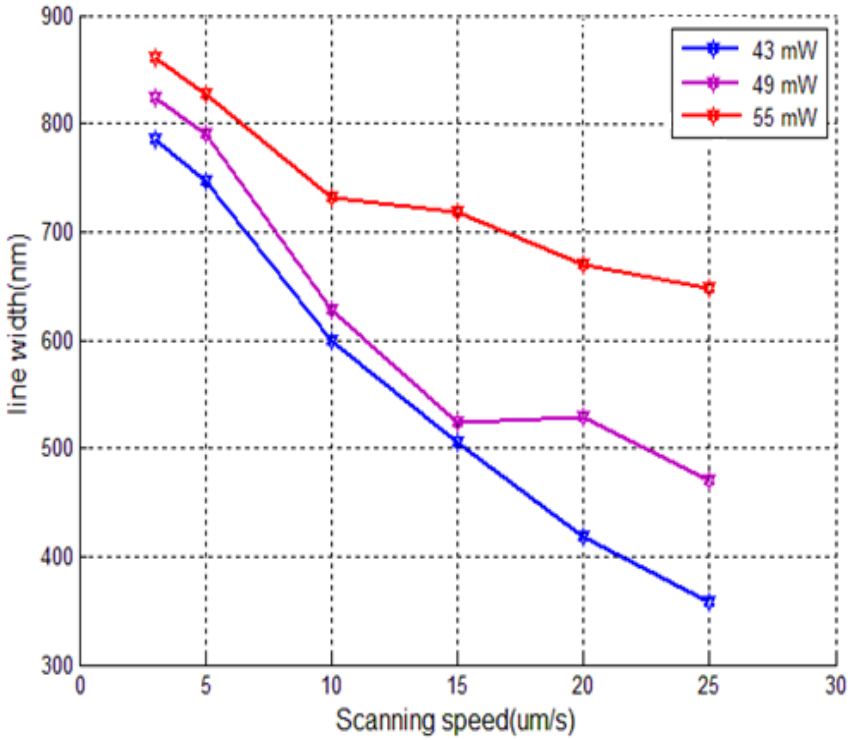

Figure 22: Variation of fabricated line widths with scanning speed at constant laser powers of 43, 49 and 55 mW.

6.4 Resolution calculation

As mentioned earlier, resolution in this study was calculated using the line array method rather than voxel array method. Numerous lines array were drawn with different scanning speeds and laser powers. The width of the line at full width at half maximum (FWHM) determines the resolution of the lithographic system. The focus of the study is on lateral resolution rather than axial resolution, although z direction is also mentioned in this chapter. Figure 23 lists the lines with mentioned line width at constant power 43 mW. The scanning speeds 3 µm/s, 5 µm/s, 10 µm/s, 15 µm/s, 20 µm/s and 25 µm/s corresponds from top to bottom line respectively.

The list of lines is followed by Bell curve shown in Figure 24. This represents the threshold power for the given lines. When the scanning speed is 3 µm/s (line width 785 nm) at the same power, the width corresponds to the full width at 5 percent of maxima. The smallest line width fabricated at this power 43 mW is 358 nm. This corresponds to FWHM. This determines the resolution of the system.

.

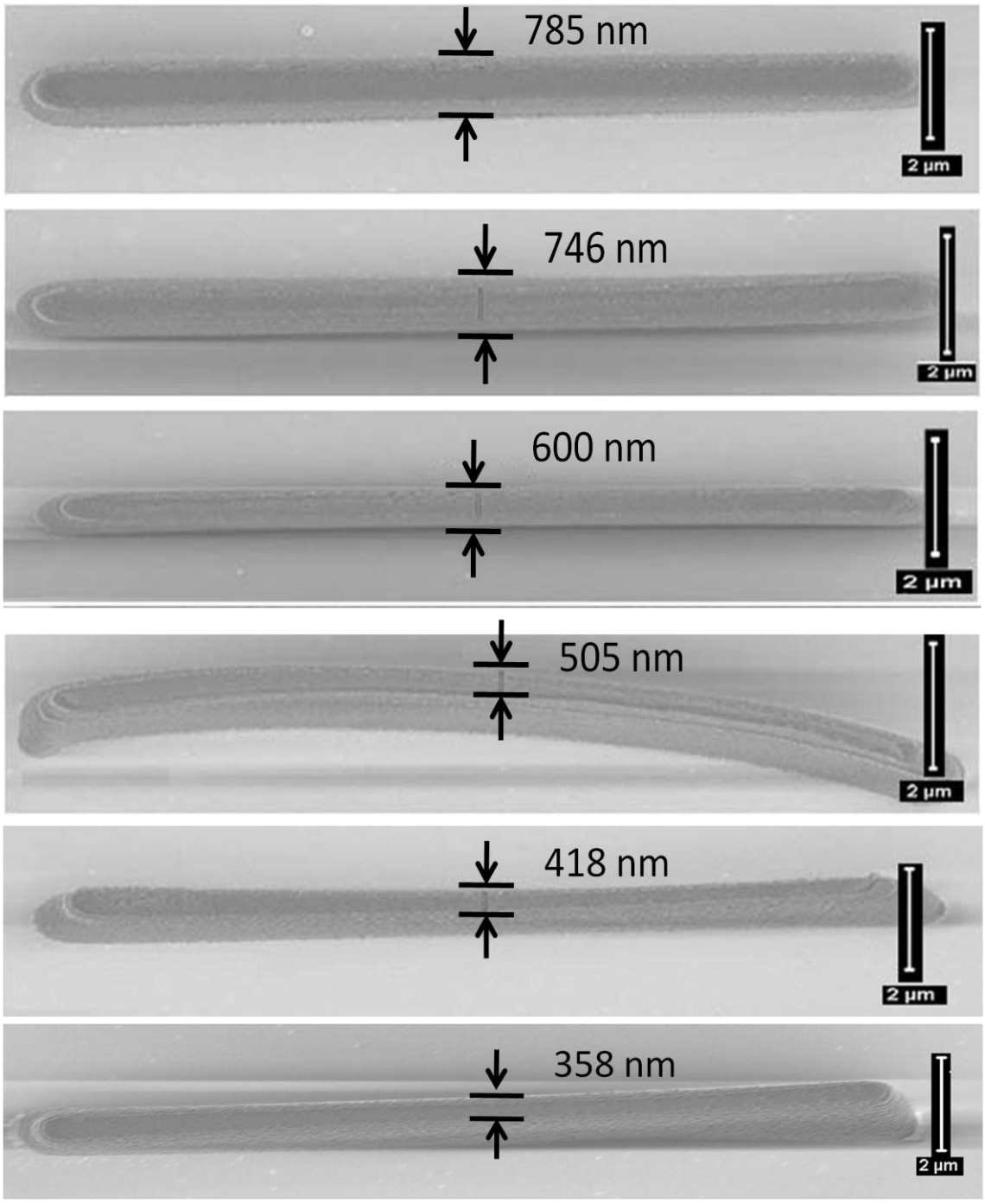

Figure 23: Lines fabricated at an incident power of 43 mW and scanning speeds of 3 µm/s, 5 µm/s, 10 µm/s, 15 µm/s, 20 µm/s and 25 µm/s (top to bottom).

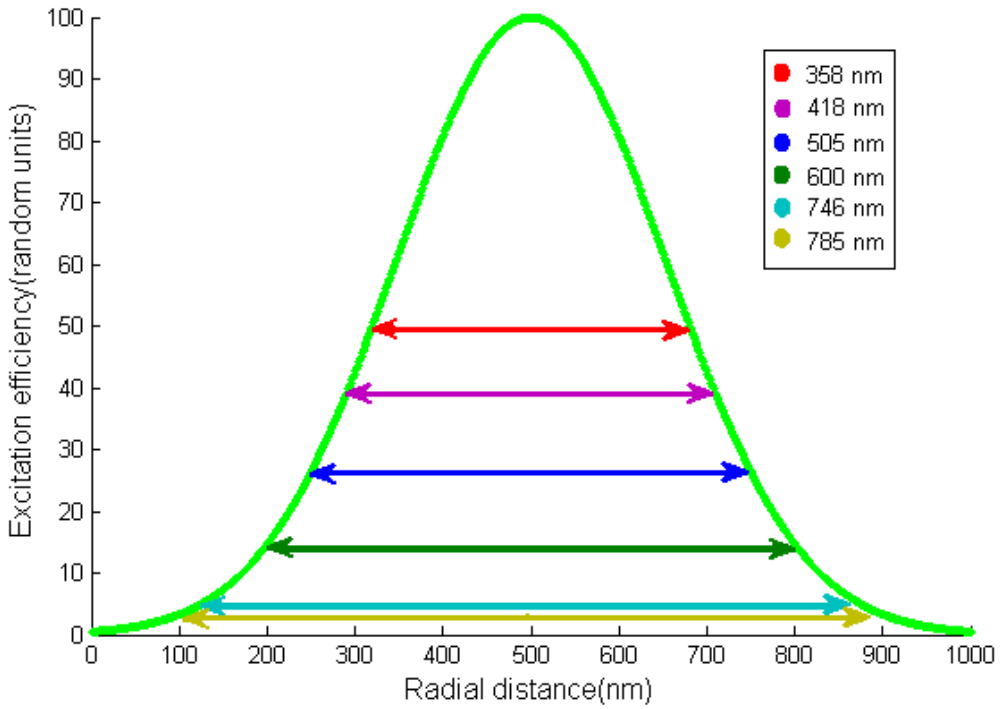

Figure 24: Gaussian curve for two photon-polymerization for resolution calculation which shows the threshold for different lines drawn at power 43 mW scanning speeds of 3 µm/s, 5 µm/s, 10 µm/s, 15 µm/s, 20 µm/s and 25 µm/s (bottom to top).

The fallen line on Figure 25 is used to measure the axial resolution. The axial resolution calculated from the Equation 9 is 3.6 µm. The height of first line, shown by Figure 24 (right) is 3.6 µm. This line is drawn at 45 mW and scanning speed 15 µm/s. For the second line on Figure 24 left (drawn at same power and scanning speed), the height is given by 3.6 um. Hence, the axial resolution shown by the figure and the calculation is equal.

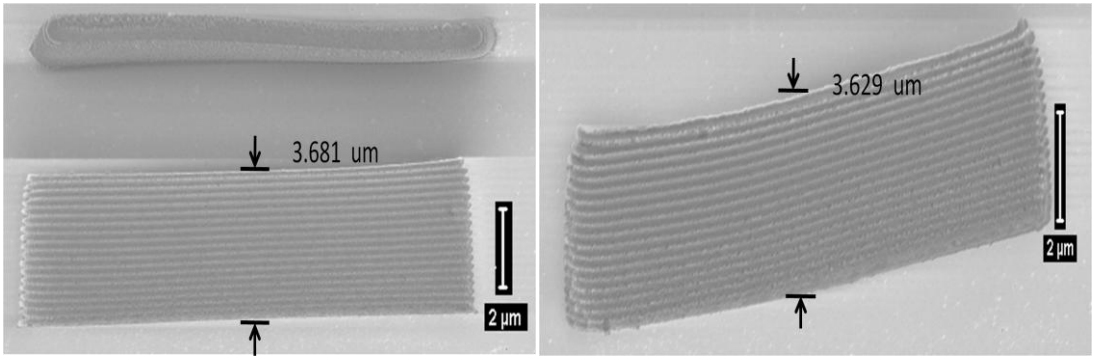

Figure 25: Measurement of height of line for the axial resolution calculation above at 45 mW and scanning speed 15 um/s below at same parameters.

6.5 Fabrication of two dimensional structures

After optimizing all the photopolymerisation parameters, the experimental setup was used to fabricate simple to complex 2D structures which includes a set of lines, lattices codes, stars, TUT logo, map of Nepal and Finland. The two dimensional lines were fabricated with power ranging from 36 to 80 mW with scanning speed ranging from 1 to 25 µm/s in the substrate of thickness 5 µm, 7 µm and 15 µm. The length of the line was 16 µm, almost same for all the lines fabricated. The width and height of the line determines the resolution which was discussed in more detail in Section 6.4. Figure 19, 22, 24, and 25 show the lines drawn at the different power and scanning speeds. As for the fabrication of the line, maximum effort was made to adjust the height of the voxel. In order to measure the height of the line, the height was adjusted in such a way that one end of voxel just touches the surface of substrate. Some of the line fell down when we fabricated several of this structure which helped us to calculate the height of the voxel. These fallen lines also give information about aspect ratio which will be discussed later. Figure 26 represents the array of line drawn at unknown power and unknown scanning speed. This was the first fabricated structure in this thesis.

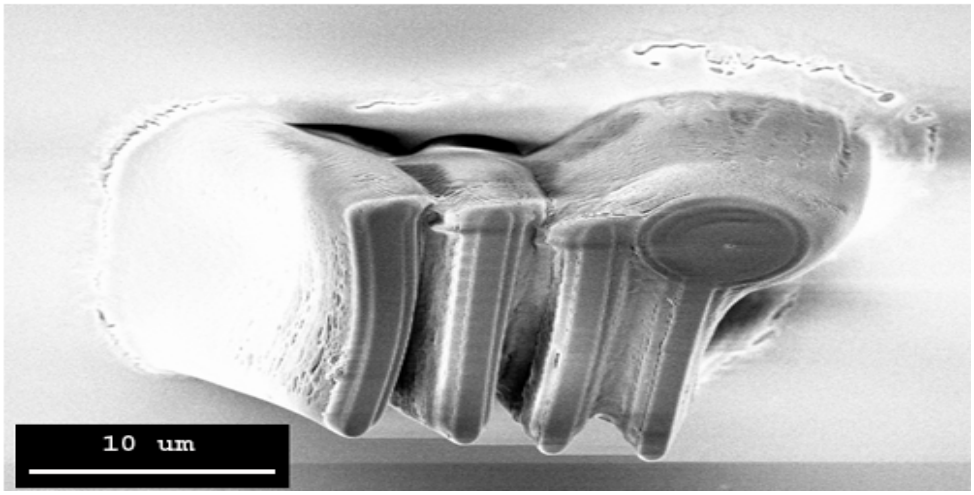

Figure 26: First fabrication: Array of lines fabricated at random speed and unknown power.

The lattice structure was drawn as the solution to the problem of collapsed line. The main idea is to support the lines by crossing the line so that the line doesn't fall. The Freeman algorithm was not implemented in fabricating these lattice structures. Simply, two triangle waveforms were employed to control the x and y coordinates in order to draw this structure. Figure 27 shows the two dimensional array of lattice structure. This figure shows that there are no broken and fallen lines. These lines within themselves provide a mechanical support to anchor each other and with the substrate. Figure b is magnified form of Figure a, where the single lattice structure is magnified. These kinds of structures not only support each other but also have practical benefits. They can be used as a tissue scaffold. This kind of lattice structure provides us basis for fabricating photonic crystal.

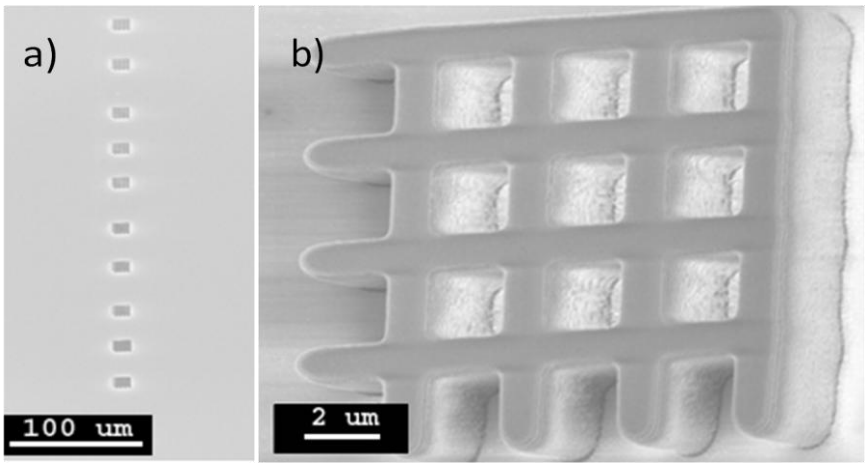

Figure 27 : a) Two dimensional array of lattice structure, showing that there are no broken or fallen lines. These lines within themselves provide a mechanical support to anchor each other and with the substrate. b) Magnified form of Figure a where the single lattice structure is focused.

Fabrication of complex structure employing the wave form is very difficult. So the Freeman algorithm was used to pattern the complex figure like a star, TUT emblem and maps. The fabrication of the star was the first implementation of vectorial scanning using the Freeman algorithm in this work. The implementation of Freeman algorithm is explained later in this section. Figure 27 shows the fabricated star. The power and the frequency adjusted for this fabrication was 43 mW and 1 Hz. The length of the star is 10 µm while the breadth of the star is 8 µm. The width of the line is 450 nm. The big dot is due to mal functioning of shutter which led to over exposure.

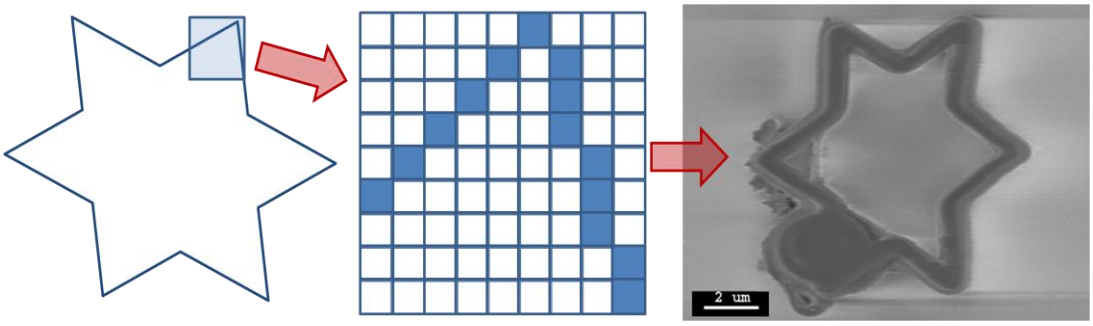

Figure 28: Fabricated star with line width of 450 nm, the length being 10 µm and width being 8 µm.

Fabrication of TUT logo is the second example of implementation of vectorial scanning which is given by Figure 29. The power and the frequency were same as mention above for fabrication of star. The length of the logo is 10.2 µm, breadth is 8 µm, and the line width is 610 nm. As compared to line width of the star the line width of TUT logo is large. The reason for this is the number of the sample point. The number of sample points that are generated by the Freeman algorithm is 2065 in the case of TUT logo while 1487 in the case of the star. So the sample has to traverse through 2065 points in 1 sec across the steady laser pointer in case of tut logo while 1487 in 1 sec in

case of star. The number of the sample point in the star is less so that the exposure time between the two points is less while the exposure time is more for the TUT logo. Similar interpretation can be done for the fabrication of map of Nepal and a line width of the map. Figure 30 shows the map of Nepal with line width of 617 nm.

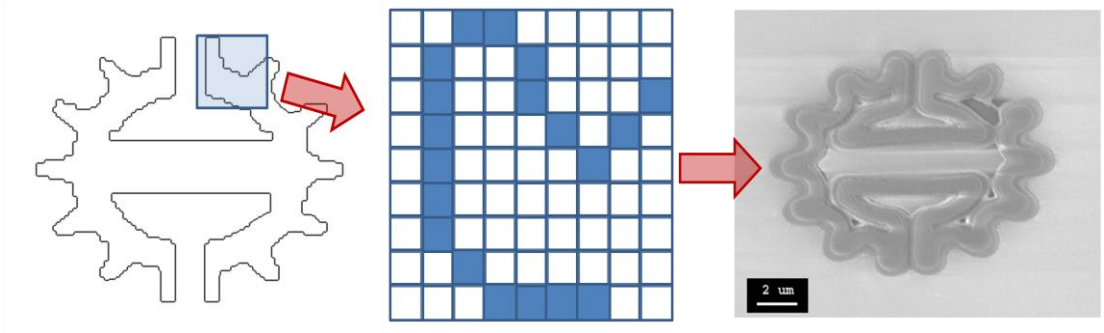

Figure 29: Fabricated TUT logo with line width of 610 nm, the length being 10.2 µm and width being 8 µm.

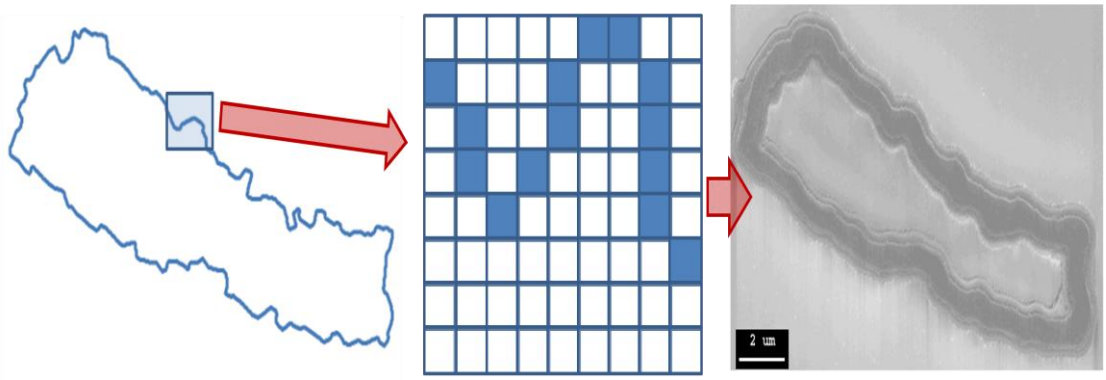

Figure 30: Fabricated map of Nepal with line width of 724 nm, the length being 16 µm.

Figure 31 illustrates the implementation of vectorial writing by utilizing vectorial Freeman chain code. The map of Finland is processed to get its outline. The outline is further processed so that there is no branched pixel in the outline. The chain code works by checking the neighboring eight pixels. After checking eight pixels, it finds the two pixels that are not empty. These two pixels are compared if they are already a code generated by the algorithm or not. Among two pixels one is already generated code which is rejected and the pointer moves to new code. This process goes on until the whole Finland map is fabricated. The Freeman algorithm is listed in the appendix.

As can be seen from the above fabricated structure the 2D contours were only fabricated by employing the Freeman vector. The Freeman algorithm can be extended to fill the space between the edges or outline of contours. Here in this thesis work 3D fabrication was avoided as the axial diameter of voxel was large.

.

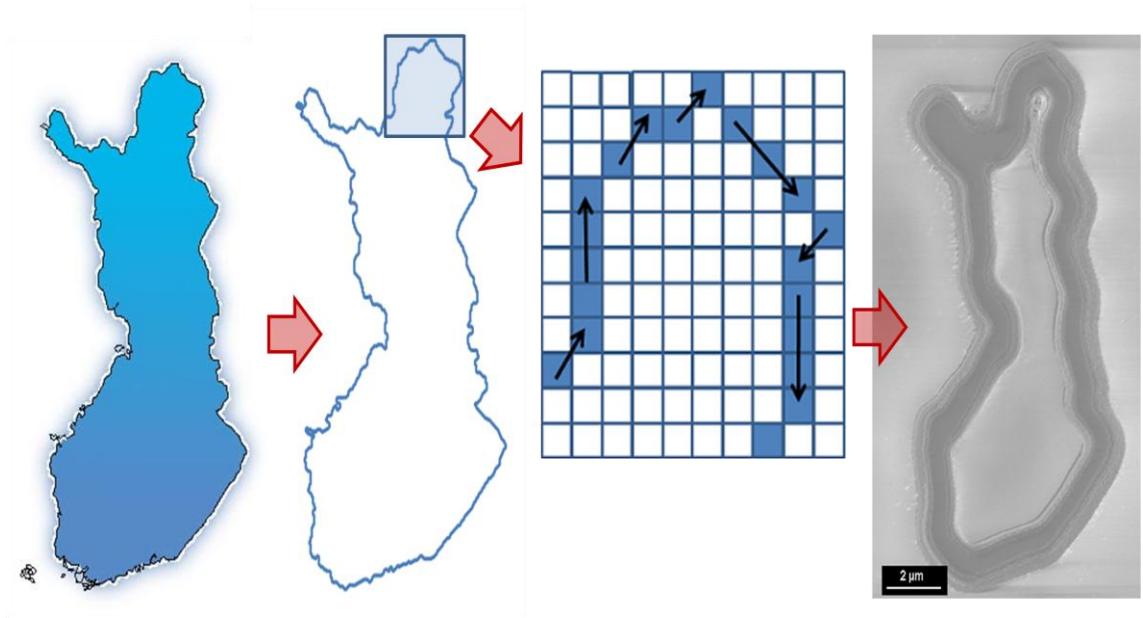

Figure 31: Illustration of implementation of vectorial scanning using freeman chain code for writing map of Finland.

6.6 Aspect ratio and reproducibility

Aspect ratio is the ratio of the height to width of the fabricated structure. The aspect ratio plays a significant role in 3D fabrication. The microstructure with the high aspect ratio falls down during development and rinsing. The two dimensional aspect ratio is studied with the help of the fabricated line of the SU-8 and is given as:

Table 3: Aspect ratio calculated from the fallen lines drawn at random thickness, random power and random scanning speed

Thickness (um)	Power (mW)	Scanning speed (um/s)	Height (nm)	Width (nm)	Aspect ratio
5	43	10	3626	518	7
5	45	15	3681	562	6.54
7	45	5	6009	758	7.92
7	53	15	7881	731	10.78
7	53	25	6376	665	9.58

Reproducibility is key feature in the manufacturing of a structure especially in companies. The lithographic system with high throughput is considered better than with low yield. This lithographic system in this thesis also has a high yield for direct laser writing. The large number of structures can be drawn with in small amount of time although this direct laser write doesn't match with the speed of fabrication by parallel TPP using spatial light modulator, micro lenses or holographic technique [78]. Figure

32 a shows the one array of lattice structure. Figure 32 b is array of tut logo. Figure 32 c is array of map of Nepal.

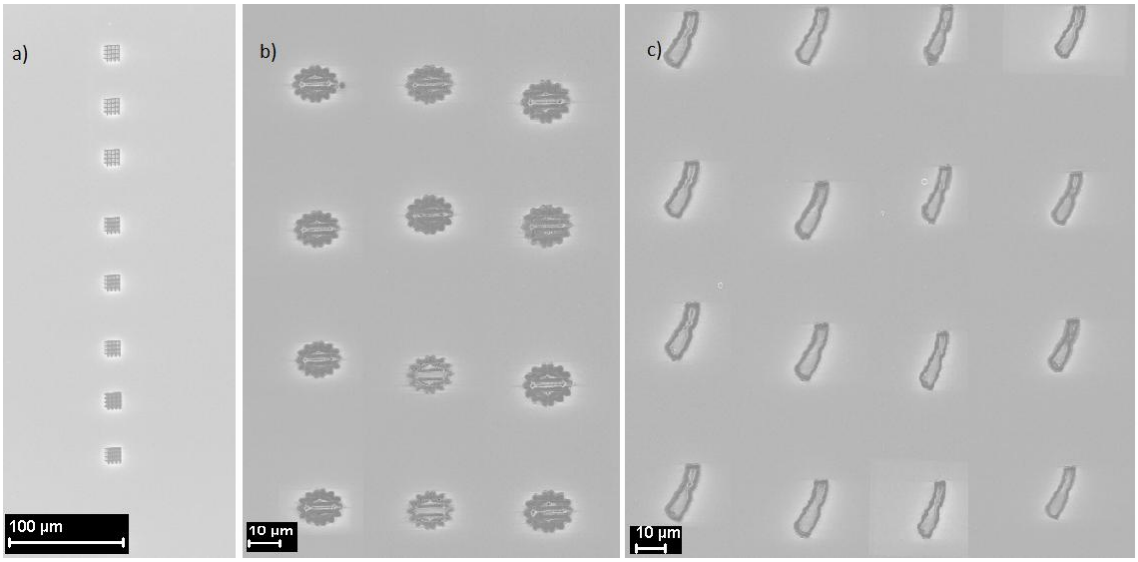

Figure 32 : arrays of fabricated structures illustrating reproducibility a) array of lattice structure b) array of TUT logo c) array of map of Nepal

7 Conclusion

Optical lithography, vertebrae of nanotechnology, has come a long way since its birth. The smallest feature fabricated 20 years back was twice the wavelength of the light beam used but today they are twenty times less. Comparison between the other forms of lithography with optical lithography showed that this lithography is behind some other lithographic techniques like electron-beam, ion-beam lithography in the term of resolution but the three dimensional fabrication capabilities surpass others. The innovation of two-photon polymerization techniques and birth of STED has promised a lot for reduction of size of structure in future. Nevertheless optical lithography has been following Moore's law to meet the demand of semiconductor industries till date.

The proof-of-principle nanofabrication was accomplished by building a two-photon photopolymerisation setup utilizing a Titanium Sapphire femtosecond laser as an excitation source. Here, SU-8, a polymeric epoxy based negative resist was used as a lithographic material and two dimensional microstructure were polymerized on the glass substrate by varying the scanning speed (exposure time) and laser power. Characterization of these patterned structures was done using a scanning electron microscope.

The thickness test showed that the fabricated structure on the thicker layer of resist was bigger in size than the thinner layer even if the laser power and the scanning speed were same. There was a significant effect seen on the size of the fabricated structure while varying the scanning speed on polymerization process. The scanning speed was varied from 3 to 25 µm/s. A slower scanning speed showed an increment in the line width while faster scanning speed showed decrement in line width. A similar effect was seen while varying the laser pulse power. At power less than threshold there was no fabrication. The threshold powers were 40 mW and 42 mW for 5 µm and 7 µm resist respectively. Slight increase in power above the threshold initiates photopolymerisation. The fine structures were drawn by adjusting the power just above the threshold power. The thickness of line increased abruptly as the power was increased. Further increment of power caused the saturation of photoinitiators fabricating constant line widths even at high powers. Different threshold powers were obtained for various thicknesses of the photoresist. It was also found that the threshold power increased as the thickness of the sample increased. Varying the scanning speed and power, lines of width ranging from 358 nm to a few micrometers were drawn.

The scanning system also plays an important role in nanofabrication. Here we demonstrated the vectorial scanning by adapting the Freeman algorithm. The raster scanning was discarded without doing any experiment as the scheme was time-consuming. Furthermore, problem of scattering of laser beam by the previously polymerized area was also considered. The experiment showed vector scanning can be

easily implemented in order to fabricate complicated structure. The map of Nepal and Finland, star, TUT logo were fabricated using vectorial writing and two-photon polymerization.

Lines with linewidth equal to FWHM were fabricated using TPP. The highest aspect ratio found in this work was 10 but the aspect ratio of SU-8 structure can exceed 20. High reproducibility was achieved in this experiment and almost every fabricated structures were developed. These exciting results in the experimental study added zeal to my effort. This work will be continued in my PhD studies where implementation of STED beam technique is expected to decrease the resolution down to 50 nm. The sub 50 nm resolution is not only related by optics but also by photoresist material. The design of this resist material system is a demand and future challenge.

References

[1] M. C. Rothch. *A road map for optical lithography*. Optics and Photonics News 21 (2010) 6, pp. 26-31

[2] J. Fischer, G. V. Freymann, and M. Wegener. *The Materials Challenge in Diffraction-Unlimited-Direct-Laser-Writing Optical Lithography*. Advanced Material 22 (2010), pp. 3578-3582

[3] L. Li, R. Gattass, E. Gershgoren, H. Hwang, J. Fourkas. *Achieving λ/20 Resolution by One-Color Initiation and Deactivation of Polymerization*. Science 324 (2009) 5929, pp. 910-913

[4] Zewail. Femtochemistry: *Atomic-Scale Dynamics of the Chemical Bond Using Ultrafast Lasers*. Angew. Chem., Int. Ed. 39 (2000), pp. 2587-2631

[5] C. N. LaFratta, J. T. Fourkas, T. Baldacchini, and R. A. Farrer. *Multiphoton Fabrication*. Angew. Chem. Int. Ed. 46 (2007) 33, pp. 6238 – 6258

[6] S. Hell. Far-field optical nanoscopy. Science 316 (2007) 5828, pp. 1153-1158

[7] J. P. Fouassier, X. Allonas, D. Burget. *Photopolymerization reactions under visible lights: principle, mechanisms and examples of applications.* Elsevier 47 (2003), pp. 16-36

[8] K. J. Schafer, J. M. Hales, M. Balu, K. D. Belfiel, E. W. Van, Stryland, D. J. Hagan. *Two-photon absorption cross sections of common photoinitiators.* Journal of Photochemistry and Photobiology 162 (2004) 2-3, pp. 497-502

[9] N. A. Jusoh and J. M. Zain. *Application of Freeman Chain Codes: An Alternative Recognition Technique for Malaysian Car Plates. IJCSNS* 9 (2009) 11, pp. 222-227

[10] C. R. Mendonca, D. S. Correa, T. Baldacchini, P. Tayalia, and E. Mazur. *A novel photoinitiator for microfabrication via two-photon polymerization*. IEEE (2006)

[11] J. Koskela. *Light induced biomaterial microfabrication for advanced cell culturing- A Comparative study*. Dissertation, Tampere. Tampere University of Technology, department of biomedical science. (2009), pp. 103

[12] D. Feng Yan, Y. Li, F. Qi, H. Yang and Q. Gong, *Reduction in feature size of two photon polymerization using SCR500,* Applied Optics Letters 90 (2007) 7

[13] H. Sun, S. Kawata. *Two-Photon Photopolymerization and 3D Lithographic Microfabrication*, Spinger-verlag 170 (2004), pp. 169-273

[14] A. Ovsianikov**,** A. Ostendorfand, B. N. Chichkov**.** *Three-dimensional photofabrication with femtosecond lasers for applications in photonics and biomedicine.* Science Direct 253 (2007) 15, pp. 6599-6602

[15] S. Klein, A. Barsella, H. Leblond, H. Bulou, A. Fort, C. Andraud, Lemercier, J. C. Mulatier, and K. Dorkenoo. *One step waveguide and optical circuit writing in photopolymerizable materials processed by two photon absorption*. Appl. Phys. Lett. 86 (2005) 21

[16] R. J. Narayana, A. Doraiswamyb, D. B. Chriseyc, B. N. Chichkovd. Medical prototyping using two-photon polymerization. Materialstoday 13 (2010) 12, pp. 42-48

[17] C. Mack (2008). *Fundamental Principles of Optical Lithography: The Science of Micro fabrication*, West Sussex:Wiley. pp 1

[18] P. B. Fischer and S. Y. Cho. *10 nm electron beam lithography and sub-50 nm overlay using a modified scanning electron microscope.* Applied Physics Letter 62 (1993) 23, pp. 2989-2991

[19] G. R. Sune, *Electron beam lithography for nanofabrication*, Phd Dissertation, Barcelona. Universitat Autonoma De Barcelona, department of fisica, (2008), pp. 20-21

[20] J. Goldstein, D. Newbury, D. Joy, C. Lyman, P. Echlin et al (2007). *Scanning electron microscopy and Xray micro analysis*. 3rd ed. New York: Springer. pp 29-47

[21] Available at http://www.news.cornell.edu/releases/july97/guitar.ltb.html on May 5, 2011.

[22] J. Rua. *Electron beam lithography throughput and resolution enhancement with innovative blanker design*. Phd Dissertation, State University of New York, (2010), pp. 265

[23] Y. Suk Kim, W. Hong, H. Joo Woo, H. Woo Choi, G. Dong kim, J. Ho Lee and S. Lee, *Ion Beam Lithography Using Membrane Masks,* Jpn. J. Appl. Phys 41 (2002) 6B, pp 4141–4145

[24] K. Arshak, M. Mihov, A. Arshak, D. McDonagh and D. Sutton. *Focused Ion Beam Lithography- Overview and New Approaches.* IEEE 2 (2004), pp. 459-462

[25] G. A. Glass, B. Rout, A. D. Dymnikov, R. R. Greco, M. Kamal, J. R. Reinhardt, John A. Peeples. *High energy focused ion beam lithography using P-beam writing.* Elsevier 241 (2005) 1-4, pp 397-401

[26] F. Watt, A. A. Bettiol, J. A. Van Kan, E. J. Teo and M. B. H. Breese. *Ion Beam Lithography and Nanofabrication, A review.* World scientific 4 (2005) 3. pp 269–286

[27] L. Scipioni. *Helium ion beam lithography in the ORION PLUS*. Available at http://www.microscopy.info/Content/pdf/Helium_Ion_Beam_Lithography.pdf at 20 July 2009

[28] J. Melngailis, A. A. Mondelli, I. L. Berry, and R. Mohondro. *A review of ion projection lithography,* J. Vac. Sci. Technol. 16 (1998) 3, pp. 927-957

[29] A. A. Tseng, *Recent Developments in Nanofabrication Using Ion Projection Lithography*, Wiley 1 (2005) 6, pp. 594–608

[30] F. Cerrina, *Wiley encyclopedia of Electrical and Electronic Engineering*. Wiley (1999), pp. 647-651

[31] K. Kise, M. Amemiya, H. Watanabe, K.Itoga, H. Yabe and H. Sumitani. *Pattern Resolution in X-ray Lithography Using Pattern Replication Technique on a Mask.* JJAP 42 (2003), pp. 3796-3801

[32] A. Heuberger. *X-ray lithography*. Sciencedirect 5 (1986) 1-4, pp. 3-38

[33] J. N. Helber (2001), *Handbook of VLSI microlithography: principles, technology and applications.* 2nd ed. New York: Noyes. pp 75-76

[34] M. Rothschild, T. M. Bloomstein, et al. *Recent Trends in Optical Lithography.* Lincoln Laboratory Journal 14 (2003) 2, pp. 221-232

[35] Zheng Cui (2008), *Nanofabrication: Principle, capabilities and Limits*, New York : Springer, pp 8-10

[36] A. Korkin and A. Z. Gilbert (2008). *Nanoelectronics and photonics*. Ottawa: Springerlink (2008) pp. 427-446

[37] A. T. S. Wee (2009), *Selected Topics in Nanoscience and Nanotechnology*. Singapore: World Scientific. pp 55-77

[38] K. Lee, R. H. Kim, D. Yang, S. H. Park. *Advances in 3D nano/micro fabrication using two-photon initiated polymerization*. Science Direct 33 (2008) 6, pp. 631-681

[39] C. W. Hull , Arcada et al. *Apparatus for production of three dimensional objects by stereolithography*. United State Patent (1986)

[40] X. Zhang, X. N. Jiang, C. Sun. *Micro-stereolithography of polymeric and ceramic microstructure.* Elsevier 77 (1999) 2 pp. 149-156

[41] C. Mack (2008). *Fundamental Principles of Optical Lithography: The Science of Micro fabrication*, West Sussex:Wiley. pp 1-3

[42] M. C. Rothch. *A road map for optical lithography*. Optics and Photonics News 21 (2010) 6, pp. 30

[43] S. Maruo, O. Nakamura and S. Kawata. *Three-dimensional micro fabrication with two-photon-absorbed Photopolymerization*. Optics Letters 22 (1997) 2, pp. 132-134

[44] S. Kawata, H. Sun, T. Tanaka, K. Takada, *Finer features for functional micro devices.* Nature 412 (2001). pp 697-698

[45] P. Arjona, G. J. de Valcarcel and E. Roldan. *Two photon absorption, Revista Mexicana de fiscal 49 (2003)*, pp. 91-100

[46] S. Kawata, H. Sun. *Two-photon photopolymerisation as a tool for making micro-devices.* Elsevier 208-209 (2003), pp. 153-158

[47] S. Wu, J. Serbin, M. Gu. *Two photon polymerization for three- dimensional micro-fabrication.* Journal of Photochemistry and photobiology 181 (2006) 1, pp 1-11

[48] H. Sun, S. Kawata. *Two-Photon Photopolymerization and 3D Lithographic Microfabrication.* Springer-Verlag (2004), pp. 187-190, 245-246

[49] R. A. Farrer, C. N. LaFratta, L. Li, J. Praino, M. J. Naughton, B. E. A. Saleh, M. C. Teich, and J. T. Fourkas. *Selective Functionalization of 3D Polymer Microstructures* Am. Chem. Soc. 128 (2006), pp. 1796-1797

[50] Y. Yagni, S. Jockush and N. J. Turro, *Photo initiated polymerization: advances challenges and oppurtunities.* Macromolecules 43 (2010) 15, pp. 6245-6260

[51] B. Boroli. *Review photo polymerization of biomaterials: issues and potentialities in drug delivery, tissue engineering and cell encapsulation application*. Wiley 81 (2006) 4, pp. 491-499

[52] J. E. Mark (2007). *Physical properties of polymer handbook*. 2nd ed., New York: Springer, pp 965-967

[53] A. Ostendorf & B. Chichkov, *Two-photon polymerization: a new approach to micromachining.* Photonics Spectra (2006), pp. 72–80

[54] T. M. Adams and R. A. Layton (2010). *Introductory MEMS*. New York: SpringerLink, pp. 66-94

[55] S. Gittard, A. Ovsianikov, N. Monteiro-Riviere, J. Lusk, et al. *Fabrication of Polymer Microneedles Using a Two-Photon Polymerization and Micromolding Process*. Journal of Diabetes Science and Technology 3 (2009), pp.304-311

[56] Z. Cui (2005). *Micro-nanofabrication: technologies and applications*. Beijing: Springer, pp 13-33.

[57] C. Mack (2008). *Fundamental Principles of Optical Lithography: The Science of Micro fabrication*, West Sussex:Wiley. pp 12-26

[58] A del Campo and C Greiner. *SU-8: a photoresist for high-aspect-ratio and 3D submicron lithography*. Journal of micromechanical and microengineering 17 (2007) 2, pp. R81-R95

[59] Nano™ SU-8, Available at http://www.microchem.com/pdf/SU8_2-25.pdf on 5 May 2011

[60] I. Zailer, J. E. F. Frost, V. Chabasseur-Molyneux, C. J. B. Ford and M. Pepper. *Crosslinked PMMA as a high-resolution negative resist for electron beam lithography and applications for physics of low-dimensional structures*. IOP Science 11 (1996) 8, pp. 1235-1238

[61] Nano™ PMMA and copolymer, Available at http://www.microchem.com/pdf/PMMA_Data_Sheet.pdf on 5 May 2011

[62] L. H. Ngayen, M. Straub, M. Gu. *Acrylate based Photopolymer for Two photon micro fabrication and photonic application.* Wiley 15 (2005) 2, pp. 209-215

[63] H. J. Kong and S. W. Yi. *Ultrafast Laser Induced Two Photon Polymerization of Su8 High Aspect ratio structure and nano wire*. Journal of the Korean Physical Society 54 (2009) 1, pp 215-219

[64] S. Aura, T. Sikanen, T. Kotialo, S. Franssila. *Novel hybrid material for microfluidics devices*. Elsevier 132 (2007) 2, pp. 397-403

[65] A. Doraiswamy, T. Patz, R. Narayan, B. Chichkov, A. Ovsianikov,R. Houbert, R. Auyeung, D.B. Chrisey. *Biocompatibility of CAD/CAM Ormocer polymer scaffold structure.* Materials Research Society 845 (2005)

[66] M. Popal, A. Dabek, M. E. Robertsson et al. *ORMOCERs - New Photo-Patternable Dielectric and Optical Materials for MCM-Packaging.* IEEE (1998), pp. 1018-1025

[67] A. Kwok-kit Wong (2001), *Resolution enhancement techniques in optical lithography, Washington:* SPIE, pp 28-30

[68] E. Hecht (2002). *Optics*. 4th ed. San Francisco: Addison Wesley, pp. 531-532

[69] Confocal laser scanning microscopy. Available at http://www.zeiss.de on 16 May 2011

[70] H.B. Sun, M. Maeda, K. Takada, J.W.M. Chon, M. Gu, S. Kawata. *Experimental investigation of single voxels for laser nanofabrication via two-photon Photopolymerization*. Applied Optics Letters 83 (2003) 5, pp. 819-823

[71] N. Uppal. *A mathematical model development and sensitivity analysis of two photon polymerization for 3d micro/nano fabrication.* Dissertation, The University of Texas at Arlington, department of mechanical engineering, 2008, pp. 156

[72] S. Wu, J. Serbin, M. Gu. *Two photon polymerization for three- dimensional micro-fabrication.* Journal of Photochemistry and photobiology 181 (2006) 1, pp 4-5

[73] S. W. Hell. *Far-Field Optical Nanoscopy*. Science 316 (2007), pp. 1153-1158

[74] J. Fischer ,M. Wegener. *Three-dimensional direct laser writing inspired by stimulated-emission-depletion microscopy.* Optical Material Express 1 (2011) 4, pp. 614-624

[75] P. Wei, N. Li, and L. Feng. *Two-Photon Polymerization System With Diffractive Superresolution Element.* IEEE 11 (2011) 1, pp. 194-198

[76] R. G. Hunsperger (2009). *Integrated Optics: Theory and technology.* Newark: Springerlink (2009), pp. 201-202

[77] N. A. Jusoh and J. M. Zain. *Application of Freeman Chain Codes: An Alternative Recognition Technique for Malaysian Car Plates.* IJCSNS 9 (2009) 11

[78] N. J. Jenness, K. D. Wulff, M. S. Johannes, M. J. Padgett, D. G. Cole, and R. L. Clark. *Three-dimensional parallel holographic micropatterning using a spatial light modulator.* Optics express 16 (2008) 20, pp. 15942-15948

APPENDIX 1: Freeman Code

```
clear all;
A=imread('C:\Documents and Settings\kunwar\Desktop\p.gif');

%selection of arbitrary pixel and its neighbor and assigning them in
%variable
b=A(84,7);
x=84;y=7;
e=85; f=7;

 for j=1:658
     i=1;

%checks the eight neighboring pixel for desired pixel and assign the
%pointer in next pixel and return two pixel position in term of x and
%y coordinates
  if((A(x+1,y+1)==40))
         c(i)=x+1;
         d(i)=y+1;
         i=i+1;
  end
  if((A(x+0,y+1)==40))
         c(i)=x+0;
         d(i)=y+1;
         i=i+1;
  end
  if((A(x-1,y+1)==40))
         c(i)=x-1;
         d(i)=y+1;
         i=i+1;
  end
  if((A(x-1,y+0)==40))
         c(i)=x-1;
         d(i)=y+0;
         i=i+1;
  end
  if((A(x-1,y-1)==40))
          c(i)=x-1;
          d(i)=y-1;
          i=i+1;
  end
  if((A(x+0,y-1)==40))
          c(i)=x;
          d(i)=y-1;
          i=i+1;
   end
   if((A(x+1,y-1)==40))
          c(i)=x+1;
          d(i)=y-1;
          i=i+1;
   end
   if((A(x+1,y)==40))
```

```
            c(i)=x+1;
            d(i)=y;
            i=i+1;
    end

%checks if the pixel position is already counted or not and returns
%the one that is not counted before
        if c(1)==e && d(1)==f
            g1=1;
        end
        if c(2)==e && d(2)==f
            g1=2;
        end
        e=x;f=y;

%store the uncounted pixel position into array and mark it as counted
and return freeman code in the form of array
        if g1==1
            m(j)=c(2);
            n(j)=d(2);
        end
        if g1==2
            m(j)=c(1);
            n(j)=d(1);
        end
            x=m(j);
            y=n(j);
end
```